Solar Energy Materials & Solar Cells 267 (2024) 112715

Contents lists available at ScienceDirect

Solar Energy Materials and Solar Cells

journal homepage: www.elsevier.com/locate/solmat

Review

Photon management in silicon photovoltaic cells: A critical review

Mohammad Jobayer Hossain [a,e,f,*], Mengdi Sun [a,g], Kristopher O. Davis [a,b,c,d]

[a] CREOL, the College of Optics and Photonics, University of Central Florida, Orlando, FL, USA
[b] Resilient Intelligent Sustainable Energy Systems (RISES) Faculty Cluster, University of Central Florida, Orlando, FL, USA
[c] Department of Materials Science and Engineering, University of Central Florida, Orlando, FL, USA
[d] FSEC Energy Research Center, Cocoa, FL, USA
[e] American Institute for Manufacturing Integrated Photonics (AIM Photonics), Albany, NY, USA
[f] The Research Foundation for State University of New York, Albany, NY, USA
[g] Bradley Department of Electrical and Computer Engineering, Virginia Tech, Arlington, VA, USA

ARTICLE INFO

Dataset link: https://doi.org/10.6084/m9.figshare.23573409.v1

Keywords:
Light trapping
Path length enhancement
Photon management
Recombination
Silicon
PV cell

ABSTRACT

With the practical efficiency of the silicon photovoltaic (PV) cell approaching its theoretical limit, pushing conversion efficiencies even higher now relies on reducing every type of power loss that can occur within the device. Limiting optical losses is therefore critical and requires effective management of incident photons in terms of how they interact with the device. Ultimately, photon management within a PV cell means engineering the device and constituent materials to maximize photon absorption within the active semiconductor and therefore reduce the number of photons lost through other means, most notably reflection and parasitic absorption. There have been great advancements in the front and the rear side photon management techniques in recent years. This review aims to discuss these advancements and compare the various approaches, not only in terms of increases in photogenerated current, but also their compatibility with different PV cell architectures and potential trade-offs, like increased surface recombination or scalability for high-volume manufacturing. In this review, a comprehensive discussion of a wide variety of the front and the rear side photon management structures are presented with suggestions to improve the already achieved performance further. This review is unique because it not only presents the recent development in photon management techniques, but also offers through analysis of these techniques and pathways to improve further.

1. Introduction

Photovoltaic (PV) energy conversion has now become one of the cheapest sources of electricity [1], less expensive than most fossil fuel-based resources. Sunlight is abundant on earth, and PV cells and modules directly convert incident photons into electricity using a process called photovoltaic effect. A wide variety of materials can be used to make PV cells, including organic semiconductors, perovskites, III-V semiconductors, chalcogenides, and of course silicon (Si). Even though some of these materials are less expensive to produce and others yield higher conversion efficiencies, crystalline Si (c-Si) has been and continues to dominate the PV manufacturing sector with a current market share of approximately 95% [2]. Si has a bandgap of 1.12 eV, which is an optimal value for a single junction PV cell based on the AM 1.5G solar spectrum. However, it has an indirect bandgap that results in weak absorption near the band edge. Other materials have direct bandgaps of a similar magnitude, so why does silicon remain the dominant material? For starters, Si is the second most abundant element on earth, behind only oxygen. Secondly, many decades worth of research, development, and production in the integrated circuits sector have led to an incredible understanding of how to work with Si and produce it at a large scale. Finally, Si-based modules have shown to be very durable and reliable over time with very low degradation rates reported from the field [3–7]. This, combined with the relatively high efficiencies obtained and the low production costs, have all contributed to the continued use of Si by PV manufacturers.

Incident photons coming from the sun serve as the "fuel source" in a PV cell. The wavelengths of these photons span the ultraviolet, visible, and infrared domains. Not all the incident photons enter the cell. As illustrated in Fig. 1, some are reflected off the front surface of the cell and others are parasitically absorbed by other front surface layers of the device. Of the photons that do enter the semiconductor, not all will get absorbed and generate an electron–hole pair. Photons with energies smaller than the bandgap either do not get absorbed at all or get absorbed and converted into heat (e.g., free carrier absorption). Others may reach the rear side of the cell and get transmitted through the

* Corresponding author at: CREOL, the College of Optics and Photonics, University of Central Florida, Orlando, FL, USA.
E-mail address: jobayer@knights.ucf.edu (M.J. Hossain).

https://doi.org/10.1016/j.solmat.2024.112715
Received 22 September 2023; Received in revised form 17 December 2023; Accepted 13 January 2024
Available online 21 January 2024

Nomenclature

PV	Photovoltaic
LCOE	Levelized cost of energy
PERC	Passivated emitter rear contact
SHJ	Silicon heterojunction
HIT	Heterojunction with intrinsic thin-layer
POLO	Polycrystalline silicon on oxide contacts
TOPCon	Tunnel oxide passivated contact
IBC	Interdigitated back contact
ARC	Antireflection coating
SN	Serial number
EQE	External quantum efficiency
DRIE	Deep reactive ion etching
WGM	Hispering-gallery modes
Al-BSF	Aluminum back surface field
DWCNT	Double wall carbon nanotube
HJ-IBC	Heterojunction interdigitated back contact
TCO	Transparent conducting oxides

device or absorbed by other rear surface layers (e.g., metal contacts). Even photons that are internally reflected at the rear surface can escape out the front. Some of these losses associated with the rear side of the cell could be addressed by making the Si substrate much thicker, but cost constraints prevent, and to a lesser extent bulk carrier recombination, prevent the use of very thick wafers.

Silicon, being an indirect band-gap material, experiences a rapid decrease in its absorption coefficient as the wavelength of the incident light approaches the band gap energy. (i.e., 1.12 eV or 1107 nm). This means that the thickness required to absorb all the photons increases rapidly with wavelength. The photon management structures play a crucial role in this scenario. In the presence of these structures, photons that are not initially absorbed by silicon in a single pass internally reflect back and forth between the front and rear sides of the cell (Fig. 1), which enhances the effective optical path. Termed 'path length enhancement', this mechanism is characterized by the ratio between the effective optical path and the physical thickness, known as the path length enhancement factor.

The efficiency of a PV cell is now one of the driving factors that governs the levelized cost of energy (LCOE). Cell manufacturing costs have gotten so low that a larger fraction of the total PV system costs can now be attributed to things like the glass and aluminum (Al) needed to make the modules, the mounting hardware, the wiring and conduit, and the installation labor. Many of these factors scale with area, so an increase in cell efficiency can yield a lower cost per watt at the system level [8]. The current world record for silicon PV cell efficiency is 26.8% [9,10] using a heterojunction structure, while the theoretical limit of such a cell, known as the Shockley-Queisser limit, is approximately 30% [11] under AM 1.5G solar spectrum. By implementing photon management techniques and minimizing losses such as recombination, resistive and reflection losses, the gap between the current efficiency levels and the Shockley-Queisser limit can be significantly reduced.

Recent advancements in photon management techniques for Si PV cells have led to improved theoretical understanding, fabrication methods, and cost reduction. The techniques range from nano-texturizing the active material to using resonators of various materials for front-side light trapping, and diffraction grating, planar metallic and dielectric layers for the rear side. These methods effectively trap light, resulting in an increase in photogenerated current density. However, these structures often come with drawbacks such as high surface recombination loss, which leads to low open-circuit voltage and fill factor, complex fabrication processes, higher contact resistivity and additional implementation costs, making them less suitable for industrial PV cell manufacturing. While many of these novel designs show promise in terms of photogenerated current density only, other performance parameters have yet to be fully explored.

Recent advancements in light trapping structures have led to a growing need for a comprehensive review of photon management in silicon PV cells within the research community. In our search for such papers, we have found several review papers on the topic, including those focusing on nanoscale photon management in silicon PV [12–14], nanostructured silicon PV [15], and thin silicon PV cells [16]. While these papers provide thorough analysis of different structures, they lack an examination of the various loss mechanisms and implementation feasibility associated with these structures. Additionally, many of these articles only focus on photon management from one side of the cell, either the front or rear. In this article, we aim to provide a comprehensive review of existing photon management schemes, with a particular emphasis on both the front and rear sides of the cell.

Silicon PV cells are diverse both in terms of how they are designed and manufactured [17–20]. This variety takes the form of different cell architectures, etching and surface preparation processes (e.g., anisotropic wet texturing [21–23], isotropic wet texturing [24–27], surface cleaning [28–34]), doping processes [35–40], materials and deposition methods for passivation layers and optical coatings [41–46], and various metallization and manufacturing processes [47–55]. The major cell architectures include: aluminum back surface field (Al-BSF) cells [56,57], the dominant architecture until recently; passivated emitter rear contact (PERC) cells [58–62], the newly emerged dominant architecture in the global market [63,64]; silicon heterojunctions (SHJ) or heterojunction with intrinsic thin-layer (HIT) cells [65–70], a high efficiency technology that has a smaller market share due to higher manufacturing costs; and polysilicon-based passivating contact cells, a concept introduced many years ago [71], but recently attracting a lot of attention and development under the name of polycrystalline silicon on oxide contacts (POLO) [72–74], monofacial poly-Si contacts (monoPoly) [75,76], or most frequently as tunnel oxide passivated contacts (TOPCon) [77–86]. The HIT and poly-Si architectures both feature carrier-selective, passivating contacts aimed at suppressing contact recombination. Other carrier-selective, passivating contact technologies exist and have their own advantages and disadvantages, but are not the focus of this review as they are still in the early stages of development. Additionally, interdigitated back contact (IBC) cells [87–89] are another cell structure that eliminates the use of metallization on the front side of the cell, thereby reducing the optical loss associated with light being reflected off these metal contacts. The IBC concept can be combined with other approaches, including heterojunctions and polysilicon-based passivating contacts to form very high efficiency cells, as in the current record holding 26.8% cell that is an IBC heterojunction [9,10,90].

In this article we consider the major photon management schemes, from the more conventional approaches, like the use of antireflection coatings (ARC), to more novel and recently developed approaches for these various cell architectures. Section 2 explains the underlying physics and materials properties that dictate the various energy conversion losses in a cell. These are categorized as optical (i.e., photons lost), recombination (i.e., charge carriers lost through recombination), resistive (e.g., voltage drop via inefficient charge transport), and selectivity, an issue typically limited to heterojunctions. Section 3 provides an up-to-date review of the major photon management approaches in terms of optical benefits, as well as their impact on recombination and resistive losses when incorporated into cells. Section 4 presents a comprehensive and objective analysis of the optical performance of the various schemes using optical simulations of the reflectance and quantum efficiency curves. Finally, Section 5 presents the overall conclusions.

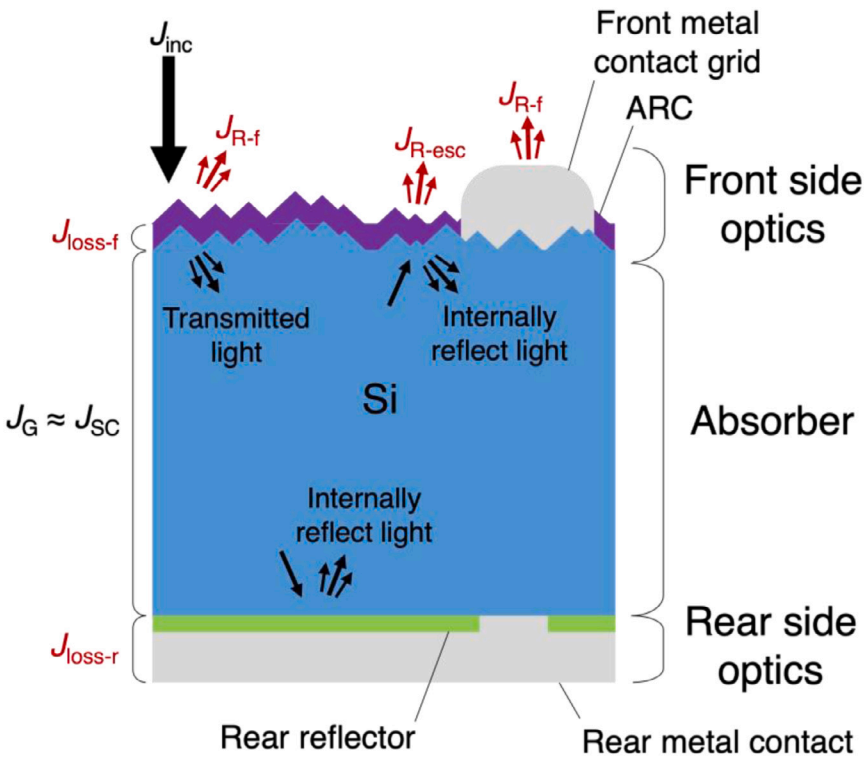

Fig. 1. Simplified illustration of the light propagation in a silicon photovoltaic cell. The figure highlights the losses in red color, including reflection and absorption losses. The legend provides a breakdown of these losses, including loss in current density due to front reflectance (J_{R-f}), loss in current density due to escape reflectance (J_{R-esc}), loss in current density (absorption) at the front side (J_{loss-f}), and loss in current density (absorption) at the rear side (J_{loss-r}). This visualization provides valuable insights into the mechanisms that affect the efficiency of the photovoltaic cell, helping to identify areas for optimization and improvement.

2. Device performance parameters and loss mechanisms in photovoltaic cells

2.1. Device performance parameters

In addition to the cell architecture selected, the efficiency of a c-Si PV cell depends on many factors, including: (1) design choices, in terms of the physical layout and dimensions of constituent components of the device (e.g., front and rear dielectric layers, metallization); (2) the materials selected to form those constituent components; and (3) the materials processing steps used to fabricate the device. Materials selection and processing dictate the composition, structure, and physical properties of the constituent components that make up the PV cell. The physical properties ultimately govern the efficiency (η), which is measured by collecting the current or current density versus voltage (I–V and J–V, respectively) of the device under standard test conditions (STC[1]). The illuminated J–V curve of c-Si PV cell can be represented fairly well as a one diode equivalent circuit using the following simplified Shockley diode equation [92] that assumes a unity ideality factor ($n = 1$) and infinite shunt resistance ($R_{SH} = \infty$):

$$J = J_G - J_0\, exp\left(\frac{V + J R_S}{kT} - 1\right). \tag{1}$$

Here, J is the current density flowing from the PV cell to the external circuit, V is the voltage at the terminals of the PV cell, J_G is the photogenerated current density, J_0 is the dark saturation current density, R_S is the series resistance of the PV cell, k is the Boltzmann constant, and T is the PV cell temperature.[2] The point of the $J-V$ curve where the product of J and V are maximum defines the maximum power current density (J_{MP}) and voltage (V_{MP}), and it is this point that defines the overall efficiency since it represents the power output of the device and the irradiance the input power. Some of the other key features of the illuminated J–V curve, often called PV cell performance parameters, include the open-circuit voltage (V_{OC}, i.e., V at $J = 0$), the short-circuit current density (J_{SC}, i.e., J at $V = 0$), and the fill factor (FF), which is simply $\frac{J_{MP}V_{MP}}{J_{SC}V_{OC}}$.

The efficiency can be expressed directly by V_{OC}, J_{SC}, and FF via the following equation, so maximizing all three is critical:

$$\eta = \frac{V_{OC}\ J_{SC}\ FF}{G_{STC}}, \tag{2}$$

where G_{STC} is the irradiance at STC and equal to 100 $\frac{\text{mW}}{\text{cm}^2}$. Beyond the maximum power point and efficiency, expressing performance in terms of these additional parameters can yield more insight into why a PV cell is performing well or not. For example, J_G and J_{SC} are typically equivalent for well-performing c-Si PV cells, and these parameters are strongly dependent on optical losses, as well as some recombination losses, in the PV cell. Because of this, J_G and J_{SC} are often the focus of many research articles reporting new photon management approaches. J_G and J_{SC} can be expressed by the following equation:

$$J_G = J_{SC} = e\int [1 - R(\lambda)]\Phi_{inc}(\lambda) IQE(\lambda) d\lambda \tag{3}$$

Here Φ_{inc} is the incident photon flux, IQE is the internal quantum efficiency, and R is the fraction of reflected light. R is the summation of both front reflectance (R_f) and the escape reflectance (R_{esc}), and both refer to the direct loss of photons (i.e., purely optical loss). R_{esc}

[1] Irradiance, G_{STC} = 1,000 W/m^2 = 100 mW/cm^2; Spectral distribution defined as air mass 1.5 global (AM1.5G) [91]; Cell operating temperature, T_{STC} = 25 °C

[2] The product of k and T is the thermal voltage and at STC, where T = 25 °C, $kT \approx 26$ meV.

refers to light that enters into the cell through front side, is not absorbed by Si, becomes reflected from the rear side, is not absorbed by Si again as it propagates back up through the Si, and then exits the cell through the front side. For a typical silicon PV cell, the total R can be measured as a function of λ using a spectrometer, and then R_f and R_{esc} can be decoupled by looking at the increase in R near the band edge, where light is weakly absorbed because of the indirect bandgap of Si [93,94]. These lost photons can be expressed in terms of lost current by multiplying each parameter by Φ_{inc} and integrating over the relevant wavelength range in a manner similar to the equation for J_G [57,95]. The resulting current densities, J_{R-f} and J_{R-esc} shown in Fig. 1, provide a quantitative measure of the impact of each on the resulting cell performance [57,96–99]. The IQE term includes both optical and recombination losses. Parasitic optical absorption does not show up in R, but nonetheless is due to a loss of photons that ultimately reduces J_G and J_{SC}. Recombination also affects the collection efficiency of carriers that are actually generated via optical absorption, but recombine before that can be extracted by the contacts.

The V_{OC} is particularly sensitive to recombination losses, and it is here where cell architectures featuring passivation, carrier-selective contacts and high quality, monocrystalline substrates really set themselves apart. Because Si is indirect bandgap, the radiative carrier lifetime is quite long (e.g., in excess of hundreds of milliseconds), so Auger and Shockley-Read-Hall (SRH) recombination losses tend to be the mechanisms that must be considered carefully when designing and fabricating c-Si PV cells. Auger recombination is strongly dependent on carrier concentration, so limiting the doping concentration as much as possible tends to be common the course of action, although this must be balanced with resistive losses. SRH recombination is ultimately the bigger concern for most PV cells. This refers to nonradiative recombination through deep-level defect states present at the surfaces and in the bulk.

V_{OC} can be expressed in various ways. By setting $J = 0$ in Eq. (1), the relationship between V_{OC} and J_0 becomes evident:

$$V_{OC} = \frac{kT}{e}\left(\frac{J_{SC}}{J_0} + 1\right). \tag{4}$$

J_0 is therefore an important figure of merit for PV cells. Minimizing SRH recombination at the surfaces and in the bulk lowers J_0, thereby increasing V_{OC}. The so called implied V_{OC} (iV_{OC}) is another way to express the V_{OC} in terms of the excess carrier concentration (Δn):

$$iV_{OC} = \frac{kT}{e}\frac{(N_{A/D} + \Delta n)\Delta n}{n_i^2}. \tag{5}$$

where $N_{A/D}$ refers to the background acceptor or donor doping concentration and n_i the intrinsic carrier concentration of the c-Si absorber. The relationship between iV_{OC} and Δn can be very useful, as it can provide a means of related carrier-related measurements like photoconductance and photoluminescence to the PV cell's V_{OC} and conversely illumination-dependent V_{OC} measurements (i.e., Suns-V_{OC}) to the injection-dependent excess carrier concentration and carrier recombination lifetimes [100,101]. Furthermore, it shows that the recombination losses effectively set a ceiling on the final V_{OC} that one can obtain. The V_{OC} cannot exceed iV_{OC}, and in most cases V_{OC} equals iV_{OC}. However, poor carrier selectivity of the electron and/or hole contacts can lead to situations where additional voltage is lost (i.e., $\Delta V = iV_{OC} - V_{OC} > 0$) [102–107]. This is particularly an issue with poorly performing heterocontacts without a homojunction present.

Finally, FF is primarily associated with the resistive elements of the equivalent circuit, particularly R_S. R_S is essentially a lumped parameter that includes many different resistive components, including the (ideally) asymmetric carrier transport to the electron and hole contact regions, charge transfer between the doped regions or TCOs to the metal contact grid or layer, current flow through the metallization, and eventually through the rest of the circuit. FF is also dependent on recombination losses [108] and carrier selectivity losses [107].

2.2. Design considerations and losses at the front side

If we consider how the cell architecture, design, materials, and resulting properties influence the overall performance, it is helpful to break the cell into the front side, bulk absorber, and rear side, as in Fig. 1. At the front, critical design elements include the surface morphology, the thickness and physical properties of any thin film layers, and dimensions, shape, and electrical properties of the front metallization grid. The surface morphology, including the size and shape of the surface texture, can impact the front surface reflectance (J_{R-f}), as well as the direction light will propagate within the c-Si absorber. This is covered in more detail in subsequent sections.

Thin films at the front surface can minimize J_{R-f} when used as a ARC or multi-layer ARCs [109–114], when a wide bandgap material is used with the appropriate refractive index and thickness. It can also increase J_{loss-f} if the materials has a significant absorption in the wavelengths of interest. This is particularly an issue for heterojunction cells (e.g., HIT) featuring doped amorphous silicon films and a TCO, like indium tin oxide (ITO) [115]. Parasitic optical absorption in the amorphous silicon layers primarily affects blue part of the spectrum, but the TCO can affect longer wavelengths and is highly dependent on the carrier concentration. The use of alternative passivating, carrier-selective contact materials with wider bandgaps and therefore less absorption has been an area of active research with various metal oxides of particular interest [102,103,116–136]. For both homojunction and heterojunction devices, the thin film in direct contact with the front of c-Si absorber should lower surface recombination by passivating interface defects that act as SRH recombination centers and preferably also lowering the minority carrier concentration at the surface [46]. For cell architectures featuring a front homojunction (e.g., Al-BSF, PERC, TOPCon), this film is typically an insulating dielectric film, whereas for heterojunctions, the film must either be conductive or thin enough to still allow the desired charge carrier to be transported through the layer.

Finally, the front metallization grid impacts the optical, recombination, and resistive losses. Optical shading from the front metallization leads to front reflectance loss (J_{R-f}) and is dependent on the fractional area covered with metal and the shape of the metal grid lines. Similarly, metal-silicon interfaces are have a very high interface defect density, and tend to yield excessively high J_0 values [137–142]. Limiting the metal contacted area seems to be prudent, but limiting it too much can lead to poor current collection and significant voltage drop at the interface [141,143,144] and along the grid lines, thereby increasing R_S and lowering FF. By printing narrow grid lines with a high aspect ratio, this can be mitigated to some extent. IBC cells obviously avoid some of these issues and trade-offs all together, but at come at a higher cost and added manufacturing complexity.

2.3. Design considerations and losses in the bulk absorber

Compared to the front and rear side, the design considerations of the bulk absorber are much simpler. Arguably the most desirable characteristic of the bulk absorber is to maximize the bulk carrier lifetime, because this sets a ceiling on the overall effective carrier lifetime of the entire device which is ultimately tied to the key recombination-related device parameters like J_0 and V_{OC}. The bulk carrier lifetime is strongly depends on the concentration of deep-level SRH defects formed by the presence of crystallographic defects within the Si lattice. This can be various point defects (e.g., impurities) and structural defects like grain boundaries and dislocation clusters. In years past, this was particularly an issue for cells made from multicrystalline (i.e., polycrystalline) silicon wafers. However, in recent years, the industry has almost completely transitioned to the use of monocrystalline silicon wafers grown using the Czochralski (Cz) method. Even with the use of Cz wafer, the dopant type (e.g., n, p), dopant species (e.g., B, Ga, P), dopant concentration, and absorber thickness remain important

design considerations. The as-grown quality of the resulting crystals and subsequent processing steps, particularly those occurring at higher temperatures and/or those that introduce significant hydrogen to the absorber are also very critical. For this review, the thickness is of particular importance because the ability to absorb the majority of the band edge photons depends on the optical path length, which is based on both the thickness and the light trapping performance of the device. As the absorber thickness gets smaller due to cost pressure associated with the crystal growth process, light trapping becomes more and more critical.

2.4. Design considerations and losses at the rear side

In terms of recombination and resistive losses, the rear side shares similar design considerations as the front. To help keep J_0 low and V_{OC} high, the rear surface should be well-passivated with limited contact between the rear metallization and the c-Si absorber. Similarly, this must be balanced with the resistive losses associated with limiting the rear contact fraction. Of course, the use of a passivating, carrier-selective contact stack at the rear can alleviate some of this tradeoff, as is the case with HIT and TOPCon cells. With regards to optical losses, the situation is quite different. Rather than limiting the front surface reflectance and broadband parasitic absorption, the primary optical considerations at the rear are to maximize the internal back reflectance [93,94,145,146] and, if possible, redirect the internally reflected light to increase the optical path length and potentially help maintain a higher reflectance for subsequent internal reflection (e.g., at the front).

Both the rear surface morphology and the properties and thickness of the rear reflectors govern the internal reflectance and the light redirection. The rear reflectors should have a low refractive index for wavelengths near the band edge, since Si has a large refractive index ($n \approx 3.5$) and a large difference in the refractive index is what yields a large internal reflectance. For random upright pyramids formed via anisotropic etching at the front side and common low index rear reflectors like silicon oxide and silicon nitride at the rear (Fig. 1), much of the light entering the c-Si absorber is transmitted at an angle in excess of the critical angle for total internal reflection. However, the rear reflector film thickness must be kept sufficiently thick (e.g., greater than 100–150 nm) to prevent energy transfer from the "transmitted" evanescent wave to the underlying metal contact [94]. The use of thinner films and lossy metals can lead to significant parasitic absorption at the rear side leading to current loss in the form of the J_{loss-r} term shown in Fig. 1.

An important consideration for both the front and rear surface is that the surface morphology of the c-Si absorber can also affect the surface recombination. Planar surfaces are much easier to passivate, whereas nanostructured surfaces can be more of a challenge. Research focused on photon management can often focus on the optical performance of novel nanostructured surfaces without consideration of how effectively the surface can be passivated. That is not to say it is impossible, in fact aluminum oxide deposited by atomic layer deposition has been shown to provide some level of passivation of nanostructured black silicon [147–156].

3. Photon management structures used in si PV

Incomplete light trapping and parasitic optical absorption are two major challenges in reaching the Shockley–Queisser efficiency limit. Various photon management techniques have been studied to address these issues, including reducing losses, enhancing the optical path, and increasing the probability of photon absorption. Fig. 2 illustrates the performance parameters and the photon management structures of numerous silicon PV cells reported recently, carefully chosen to represent most of the cell types, photon management structures and surface passivation conditions. Here, the overall efficiency (η) is represented by the colorbar. The V_{OC} and J_{SC} of the cells are shown in X and Y axis respectively, and their performance parameters are listed in Table 1. The shape of the data points in the figure represents the front side photon management structures, and a white circle inside some of the data point means that their rear side is structured (i.e., not planar). The label of the data points includes the cell type and their serial number (SN) on Table 1. The vertical and horizontal dotted lines represent the maximum V_{OC} and J_{SC} values attainable from a c-Si PV cell respectively. The data samples are discussed in detail in the following subsections, providing a summary and evaluation of the optical and electrical performance of these PV cells in relation to various photon management approaches.

3.1. Front side structures

Various methods have been utilized to improve the transparency of the photovoltaic cells on the front side, such as applying an antireflective coating (ARC), texturing the surface, and utilizing resonators. A graphical representation of these techniques is presented in Fig. 3(a).

Single layer dielectric antireflective coating (ARC) is a straightforward method to reduce reflection losses. Silicon Nitride (SiN_X) is commonly used as the coating material [158,159] due to its lower refractive index (≈2) than crystalline silicon (≈4). Single layer ARC has the potential to achieve 100% optical transmission at the corresponding wavelength. Due to its simple fabrication process and low cost, dielectric ARC is widely used in commercial PV cells. However, it should be noted that the optical performance of single layer ARC is dependent on wavelength and polarization, and it has limited angular optical response which can be a drawback in practical applications [160].

To broaden the spectral and angular responses of ARC, various strategies have been examined. These methods can currently be divided into two categories: patterning on layers with different materials and direct patterning on the silicon wafer (surface texturing). In these architectures, nano or microstructures with gradually varying geometries are positioned above the silicon wafer, resulting in higher transmission. Unlike traditional single layer ARC, these approaches exhibit an omnidirectional and broadband optical response due to the graded index distribution and thus destructive interference of a wide range of wavelengths, which is crucial for PV cells.

Antireflective nanostructures with different shapes have been studied, including nanowires, nanopillars, nanodomes, nanospheres, nanorods, and nanocones. For example, Jeong et al. investigated the performance of an ultra-thin silicon nanocone PV cell [161]. In this study, Si nanocones were fabricated on top of a Si substrate, and interdigitated Al contacts were placed on the rear side to prevent shadowing losses. The cell demonstrated 80% external quantum efficiency (EQE) in the 400–800 nm wavelength range, and a J_{SC} of 29 mA/cm^2. Here, in addition to the antireflection effect, enhanced light scattering from these structures also contributed to the light trapping. Cordaro et al. nanopatterned the SiN_X ARC layer, which provided with a boost of 2.3 mA/cm^2 in the J_{SC} in comparison with the planar ARC [162]. Nanowires are another effective geometry in light management. Lee et al. reported a radial junction PV cell with hybrid silicon wire structures [163]. In this configuration, p–n junctions were formed along the radius of silicon microwire arrays. The n-type microwires were deposited on a thick silicon wafer while p-type nanowires were deposited on top of them. This design shortened the traveling path of the charge carriers, thus reducing recombination losses. The combined effects of graded index structures and light trapping between the wires significantly reduced reflection losses, resulting in an excellent 97% absorption of light and 39.5 mA/cm^2 J_{SC}.

Surface texturing is a widely used method of reducing front-side reflection losses. The main difference between surface texturing and antireflective nanostructure is that surface texturing is directly etched or deposited on the substrate, without adding a new layer with different materials. Therefore, surface texturing has a simple fabrication

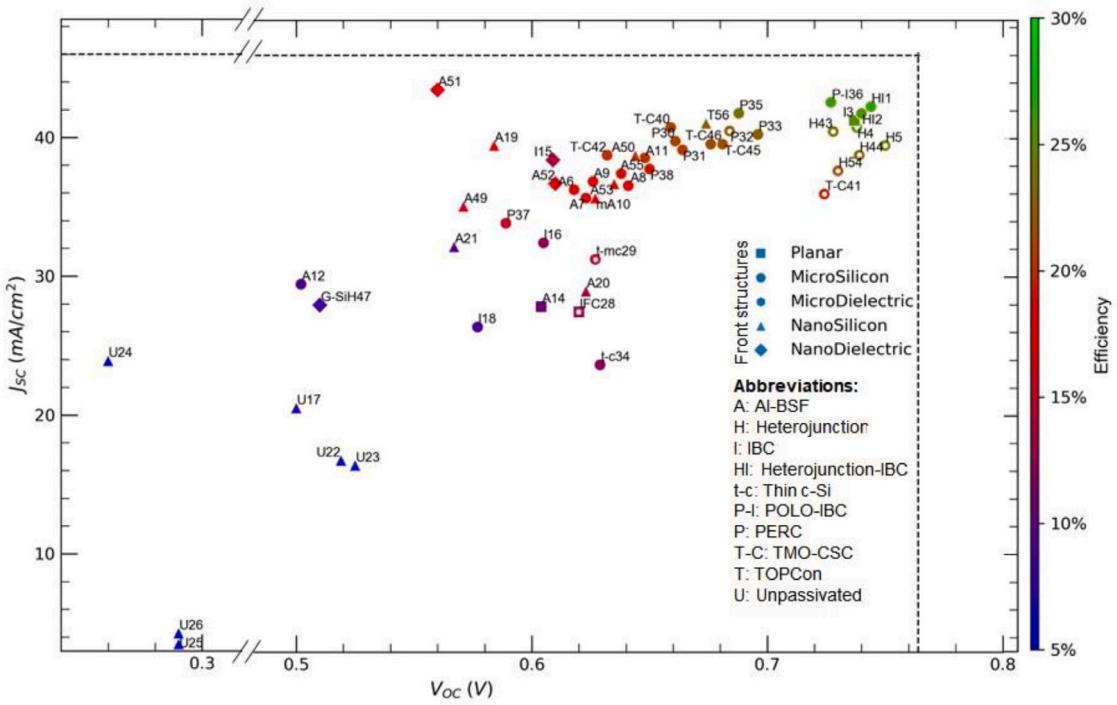

Fig. 2. Impact of front side photon management structures and cell types on the short-circuit current density (J_{SC}), open-circuit voltage (V_{OC}), and efficiency of silicon photovoltaic cells. The horizontal and vertical dotted lines represent the highest achievable J_{SC} and V_{OC} values, respectively. Performance parameters for each cell are provided in Table 1, and the data point annotations in the figure correspond to the cell types and the serial numbers in that table.

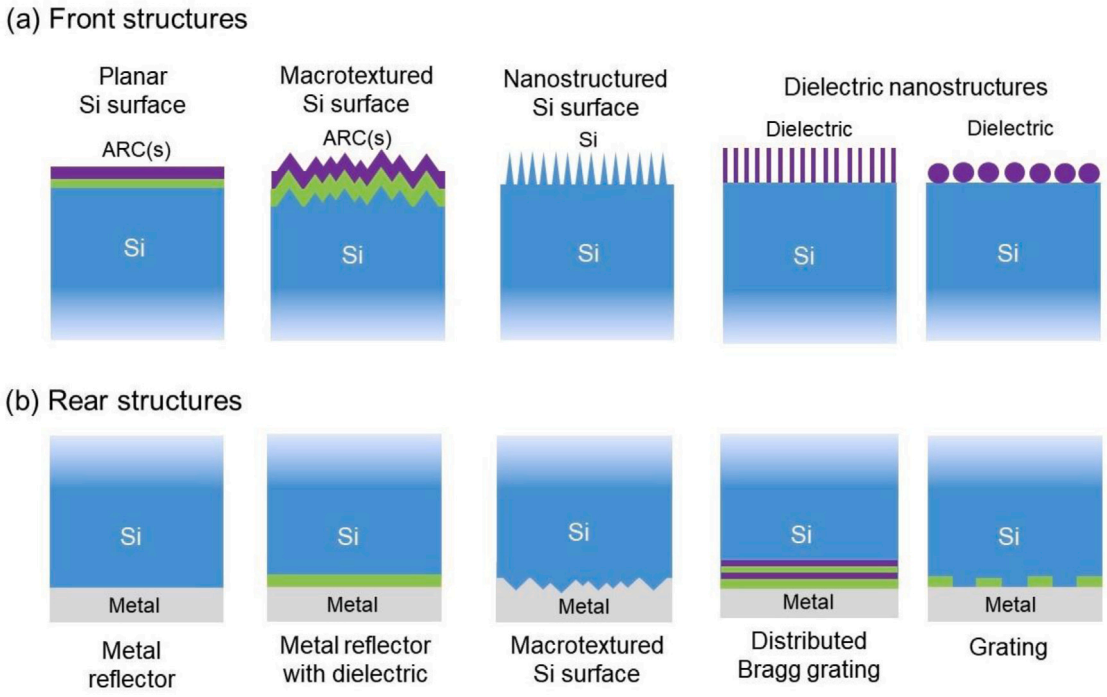

Fig. 3. Schematic representation of different photon management structures employed on the front and rear sides of a silicon solar cell. *Source:* Reproduced from [157].

process. Similar to antireflective nanostructures, enhanced transmission into the cell is achieved through altered internal angles and graded refractive index caused by gradually varying geometry. For example, Kafle et al. [164] reported a nanotextured multicrystalline (mc-Si) PV cell achieving 36.7 mA/cm^2 J_{SC}. Fellmath et al. reported another Al-BSF cell with pyramid texturing on the front surface [165] which achieved an improved J_{SC} of 38.6 mA/cm^2. A cost-effective form of nanostructured silicon called black silicon (b-Si) due to its extremely low reflection, is another candidate for excellent light trapping. It can maintain a very high transparency characteristics along a wide wavelength range, especially in the visible and infrared region, resulting in a high efficiency. Savin et al. reported a b-Si PV cell with no front-side

contact but interdigitated back-contact (IBC) that mitigated reflection losses on the front side [166]. Due to the needle-like silicon textures with high aspect ratio, an effective medium was formed resulting in a huge reduction in the front-side reflection loss. The cell achieved a very high J_{SC} of 42.2 mA/cm^2. Other applications of b-Si include ultra-thin IBC cells [167], and TOPCon cells with passivated b-Si [168].

An interesting approach of improving photon absorption in the device involves the use of optical resonators. When nanoparticles are embedded inside the PV cell, the field distribution becomes highly confined in the active layer which enhances the absorption of the incident photons. However, unwanted plasmonic absorptions can be induced by metallic nanoparticles [169]. Various materials have been adopted as nano resonators, including dielectric (Mie resonance) and metallic (plasmon resonance) materials. By applying particles with different sizes, multiple resonant peaks are excited, resulting in a broadband optical response. Additionally, these nanoparticles also scatter light, extending the optical path length inside the active region. For instance, Yao et al. [170] reported a nanoshell PV cell where a layer of silicon nanospheres helped the transfer of light to the cell through whispering-gallery modes (WGMs) [171,172]. The cell demonstrated a J_{SC} of 20.1 mA/cm^2.

3.2. Rear side structures

In the absence of a rear side photon management strategy, the light that was not fully absorbed by silicon may exit the cell, leading to a lower J_{SC}. A simple way of redirecting these photons to the active region involves using a planar metal contact (similar to the illustration in Fig. 3(b): Metal reflector) that reflects light in addition to collecting the photogenerated carriers to the external circuit. However, when incident light falls perpendicularly on a planar metal contact (e.g., Al), it is reflected perpendicularly, resulting in a path length enhancement factor of only two. Instead, if the incident light falls on the planar rear side at an angle (as in Fig. 1), which is the case when a textured front side photon management technique is used, the rear side also reflects at an angle. With that, the unabsorbed photons keep bouncing back and forth between the front and the rear side of the cell, ensuring a big boost in the path length enhancement factor. However, the unpassivated metal–semiconductor boundary acts as a recombination center which annihilates some of the photogenerated carriers before being collected to the external circuit, lowering J_{SC} and V_{OC}. Additionally, the metal contact in the rear side can also cause parasitic optical absorption loss, especially in the longer wavelengths, hurting the performance further [64,145]. One solution of this problem is to form an Al-Si eutectic, (also called back surface field or BSF) which keeps the minority carriers away from the high-recombination rear surface, also acts as a reflector. Several versions of the Al-BSF cells can be found in the literature: full-area Al-BSF, local Al-BSF, and special structures. For instance, Vermang et al. [158] reported full-area Al-BSF, blistered Al-BSF and local Al-BSF demonstrating 35.7, 36.9 and 38.7 mA/cm^2 J_{SC} respectively. The improvement in performance in these cells came from the enhanced rear-side reflection and improved surface passivation. In PERC cells, although the main purpose of the dielectric layer (i.e., Al_2O_3) in the rear-side metal–semiconductor boundary was surface passivation, it also helps increase the rear-side reflection [217] by reducing the unwanted metallic-absorption loss in the longer wavelengths [64,145]. For example, Hannebauer et al. reported a commercial PERC cell structure [218] with a J_{SC} of 39.8 mA/cm^2. The rear side photon management technique of all the cell falls into the category of planar metal reflector with dielectric in Fig. 3(b).

When it is very common to have a planar rear side (like most of the cells in Table 1), other type of structures are also used for the photon management in the rear side. Microscale structures, nanoscale structures (e.g., nanocones, nanodomes), distributed Bragg grating, and 2-D grating are examples of such structures. For instance, Zhu et al., used nanocone back reflectors in a-Si:H PV cells [188]. In this study, a-Si nanocones in the scale of hundreds of nanometers were deposited on the substrate with the same material, forming periodic nanodome structures. This structure provided scattering which helped enhance the optical path length and improved absorption in the active region. The design yielded a J_{SC} of 17.5 mA/cm^2. Also, in a recent work, Cordaro et al. used nanopatterned metal reflector engineered to suppress plasmonic loss and promote scattering [219].

Grating structures have been used on the rear side of a cell due to their ability to support resonant modes and scatter light. For example, Zeng et al. [189] reported a hybrid grating-photonic crystal back reflector silicon PV cell. The design included a reflection grating on the rear side of the cell and a 1D distributed back reflector (DBR) layer beneath the grating. The DBR achieved over 99.8% reflectance in the wavelength range of 800–1100 nm. This design resulted in a J_{SC} of 27.5 mA/cm^2.

Resonant modes have also been shown to improve light trapping on the rear side of a PV cell. For instance, Tu et al. reported the use of a double wall carbon nanotubes (DWCNTs) in amorphous silicon (a-Si) PV cells [179]. The DWCNTs were spin-coated on Ti/Ag back contacts to excite plasmon resonances and enhance light scattering in the range of 589–700 nm. The reported V_{OC} and J_{SC} were 0.83 V, and 14.07 mA/cm^2 respectively, yielding an efficiency of 6.55%

3.3. Photon management structures not yet incorporated in a practical PV cell

Recent literature presents various photon management structures grown on isolated substrates or simulated, such as Heidarzadeh et al.'s idea for increasing photogenerated current in thin-film PV cells [220] using hemispherical core–shell nanoparticles on the front and triangular grating reflectors on the rear which achieved J_{SC} of 22 mA/cm^2. The forward scattering of the core–shell nanoparticles is a positive aspect for J_{SC} but they incur plasmonic absorption, causing dips in the active material's absorption spectra and not fully utilizing the incident sunlight. Comparing this to our SunSolve simulation of planar Si and no ARC (1-R characteristics in Fig. 4(a)), it showed better absorption in Si for some wavelengths but poorer in others. However, it underperforms compared to our planar Si and ARC simulation. Therefore, using these core–shell nanoparticles does not significantly improve cell performance.

In a similar design, trapezoidal pyramid nanostructure (i.e., nanosilicon) are proposed for the front side and inverted pyramid nanotexture (i.e., nanosilicon) for the rear side of a 0.9 μm thick c-Si/ZnO heterojunction PV cell [221]. The simulations resulted in a J_{SC} of 41.94 mA/cm^2, with a front reflectance of ≤5% for 400–1000 nm wavelength and higher for other wavelengths. Although the results are promising, it is challenging to implement the nano-trapezoidal Si texture on the front side and passivate both sides, particularly the rear side where Si inverted pyramids are filled with Al.

Recently, Wang et al. has developed a ZnO nano-needle array (i.e., nanodielectric structure) for front-side photon management [222] on a textured Si substrate, which has been experimentally shown to reduce front reflectance to ≤8% at 400–1000 nm wavelength. This structure achieved a J_{SC} of 37.8 mA/cm^2, an increase of 1.8 mA/cm^2 compared to textured Si front surface. The advantage of this structure is that it avoids the challenge of passivating a nanostructured Si while providing similar front reflectance. Another similar front structure is AZO (Al doped ZnO) nanorods which experimentally provided a front surface reflectance of about 12% at 400–900 nm wavelength [223].

Saravanan et al. designed a 1-D photonic crystal (i.e., a distributed Bragg grating) for the rear side of an a-Si PV cell [224], which consisted of alternating layers of Si and SiO_2 and had the potential to make the rear side reflectance near perfect. However, it is unclear how rear side contacts could be formed through this dielectric reflector.

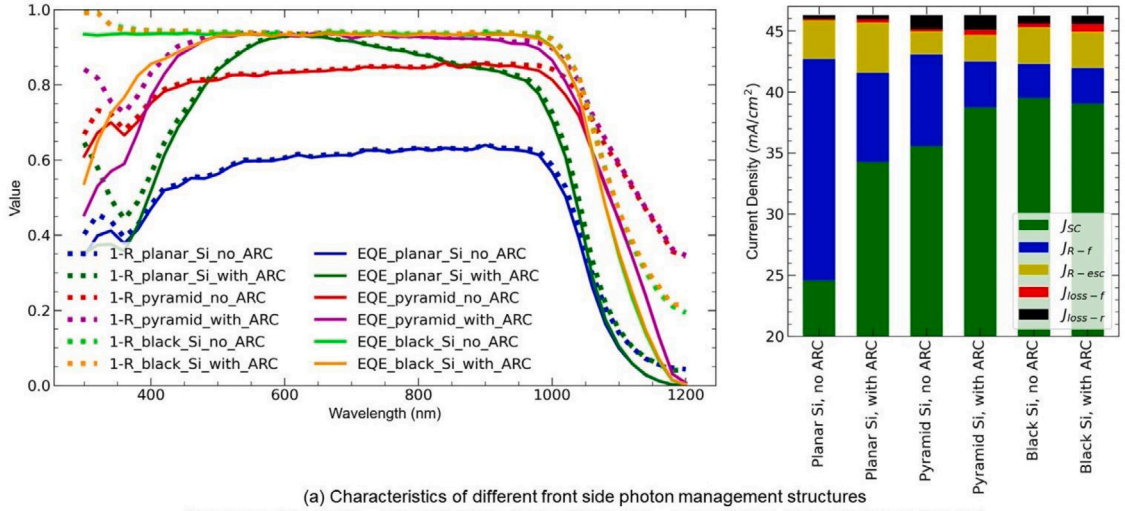

(a) Characteristics of different front side photon management structures
(fixed rear side: PERC - 1um AlSi+10nm Al_2O_3+100 nm SiN_X, no scattering. Wafer thickness: 175 μm)

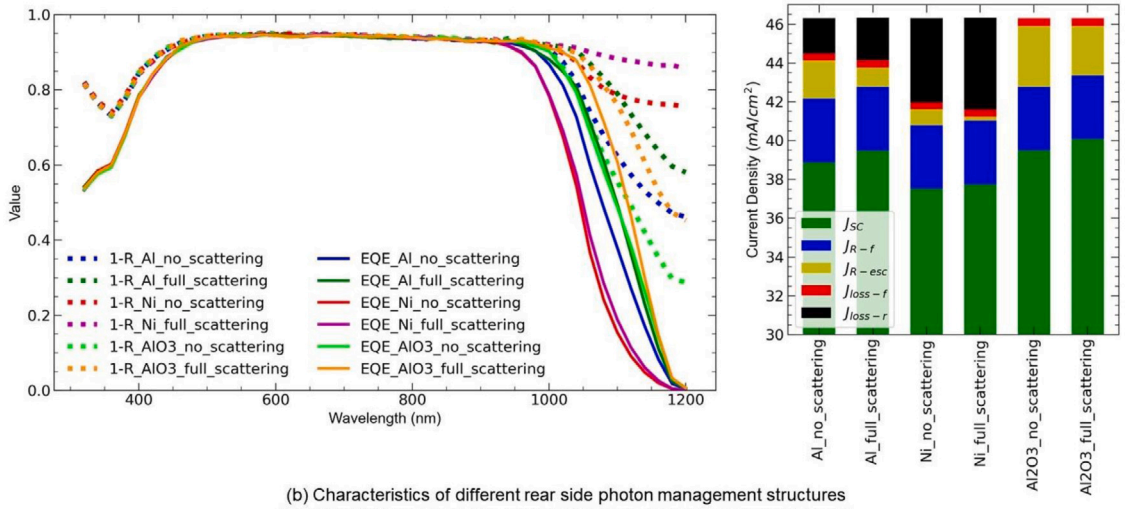

(b) Characteristics of different rear side photon management structures
(fixed front side: 75nm SiN_X + pyramid texture. Wafer thickness: 175 μm)

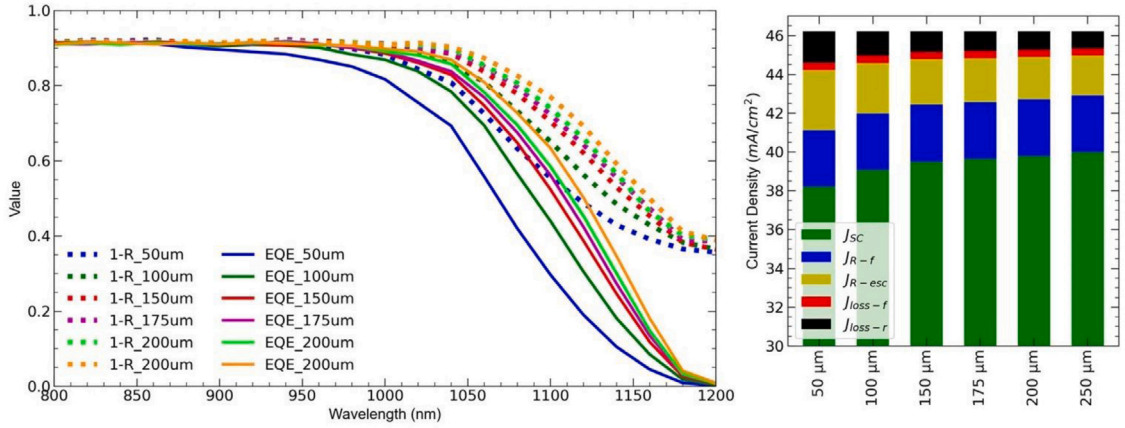

(c) Impact of cell thickness on photon management (Front: 5 μm high random pyramid, 87.5° (black Si), no ARC
Rear: PERC - 1 um AlSi contact + 10 nm Al_2O_3+ 100 nm SiN_X, full scattering)

Fig. 4. Assessment of the impacts of photon management structures on cell performance. Legend: J_{SC}: short-circuit current density, J_{R-f}: loss in current density due to front reflectance, J_{R-esc}: loss in current density due to escape reflectance, J_{loss-f}: loss in current density (absorption) at the front side, and J_{loss-r}: loss in current density (absorption) at the rear side.

Table 1
Cell performance parameters.

SN	Front structure	Rear structure	Thickness of Si (μm)	Cell type	V_{OC} (V)	J_{SC} (mA/cm^2)	FF (%)	Efficiency (%)	Reference
1	MicroSi	Planar	165	Heterojunction-IBC	0.744	42.3	83.57	26.3	[173]
2	MicroSi	Planar	150	Heterojunction-IBC	0.74	41.8	82.76	25.6	[174]
3	MicroSi	Planar	130	IBC	0.737	41.3	82.79	25.2	[175]
4	MicroSi	MicroSi	160	Heterojunction	0.738	40.8	83.36	25.1	[176]
5	MicroSi	MicroSi	98	Heterojunction	0.75	39.5	83.37	24.7	[177]
6	MicroSi	Planar	180	Al-BSF	0.618	36.3	79.34	17.8	[159]
7	MicroSi	Planar	150	Al-BSF	0.623	35.7	75.53	16.8	[158]
8	MicroSi	Planar	150	Al-BSF	0.641	36.6	77.58	18.2	[158]
9	MicroSi	Planar	150	Al-BSF	0.626	36.9	75.76	17.5	[158]
10	NanoSi	Planar	195	mAl-BSF	0.627	35.7	80.41	18	[164]
11	MicroSi	Planar	225	Al-BSF	0.648	38.6	80.36	20.1	[165]
12	MicroSi	Planar	75	Al-BSF	0.502	29.5	62.39	9.24	[178]
13	Planar	NanoDi	0.450	Thin-aSi	0.83	14.07	56.08	6.55	[179]
14	Planar	Planar	280	Al-BSF	0.604	27.9	62.31	10.5	[180]
15	NanoDi	Planar	–	IBC	0.609	38.45	59.96	14.04	[181]
16	MicroSi	Planar	–	IBC	0.605	32.48	65.19	12.81	[181]
17	NanoSi	Planar	10	Unpassivated	0.5	20.59	69.84	7.19	[182]
18	MicroSi	Planar	–	IBC	0.577	26.42	58.84	8.97	[181]
19	NanoSi	Planar	200	Al-BSF	0.584	39.5	76.29	17.6	[163]
20	NanoSi	Planar	10	Al-BSF	0.623	29	75.83	13.7	[161]
21	NanoSi	Planar	–	Al-BSF	0.567	32.2	52.09	9.51	[183]
22	NanoSi	Planar	20	Unpassivated	0.519	16.82	60.71	5.3	[184]
23	NanoSi	Planar	8	Unpassivated	0.525	16.45	55.93	4.83	[184]
24	Planar	Planar	–	Unpassivated	0.26	23.9	54.71	3.4	[185]
25	Planar	Planar	0.225	Unpassivated	0.29	3.5	49.26	0.5	[186]
26	Planar	Planar	–	Unpassivated	0.29	4.28	37.06	0.46	[187]
27	NanoSi	NanoSi	0.280	Thin-aSi	0.75	17.5	44.95	5.9	[188]
28	Planar	MicroSi	675	IFC	0.62	27.5	77.42	13.2	[189]
29	MicroSi	NanoSi	20	Thin-mcSi	0.627	31.3	77.45	15.2	[190]
30	MicroSi	Planar	–	PERC	0.661	39.8	80.58	21.2	[191]
31	MicroSi	Planar	–	PERC	0.664	39.18	79.95	20.8	[192]
32	MicroSi	MicroSi	–	PERC	0.684	40.54	81.54	22.61	[193]
33	MicroSi	Planar	–	PERC	0.696	40.3	81.28	22.8	[58]
34	MicroSi	Planar	–	TMO-CSC	0.629	23.7	82.51	12.3	[194]
35	MicroSi	Planar	180	PERC	0.6879	41.81	82.85	23.83	[195]
36	MicroSi	Planar	290	POLO-IBC	0.727	42.6	84.27	26.1	[196]
37	MicroSi	Planar	10	PERC	0.589	33.9	78.63	15.7	[197]
38	MicroSi	Planar	43	PERC	0.65	37.8	77.74	19.1	[198]
39	MicroSi	Planar	180	TMO-CSC	0.659	40.8	79.22	21.3	[199]
40	MicroSi	MicroSi	200	TMO-CSC	0.7242	36	74.03	19.3	[200]
41	MicroSi	Planar	200	TMO-CSC	0.632	38.8	81.97	20.1	[201]
42	MicroSi	MicroSi	230	Heterojunction	0.728	40.5	81.09	23.91	[202]
43	MicroSi	MicroSi	150	Heterojunction	0.739	38.8	80.60	23.11	[202]
44	MicroSi	Planar	155	TMO-CSC	0.681	39.6	80.84	21.8	[203]
45	MicroSi	Planar	175	TMO-CSC	0.676	39.6	80.69	21.6	[204]
46	NanoDi	Planar	20	Gr-Si Heterojunction	0.51	28	61.62	8.8	[205]
47	NanoDi	Planar	> 0.032	Thin-aSi	0.885	9.24	60.90	4.98	[206]
48	NanoDi	Planar	50	Al-BSF	0.571	35.11	79.21	15.88	[207]
49	NanoSi	Planar	–	Al-BSF	0.644	38.77	79.30	19.8	[208]
50	NanoDi	Planar	–	Al-BSF	0.56	43.5	68.14	16.6	[209]
51	NanoDi	Planar	–	Al-BSF	0.61	36.75	74.90	16.79	[210]
52	NanoSi	Planar	200	Al-BSF	0.635	36.74	79.81	18.62	[211]
53	MicroSi	MicroSi	200	Heterojunction	0.73	37.67	79.42	21.84	[212]
54	MicroSi	Planar	200	Al-BSF	0.638	37.47	78.93	18.87	[213]
55	NanoSi	Planar	–	TOPCon	0.674	41.1	80.50	22.3	[214]
56	NanoSi	Planar	170	TOPCon	0.696	41.44	81.69	23.55	[168]
57	MicroSi	MicroSi	–	TOPCon	0.717	40.57	84.52	24.58	[215]
58	MicroSi	MicroSi	130	Heterojunction	0.751	41.45	86.07	26.8	[90]
59	MicroSi	Planar	–	PERL	0.706	42.7	82.8	25.0	[216]

Elaboration: MicroSi=microscale silicon, NanoSi=nanoscale silicon, NanoDi=nanoscale dielectric.

Hossain et al. experimentally demonstrated the potential of self-assembled Al_2O_3 nanostructures for both surface passivation and photon management in the rear side, achieved through suppression of parasitic optical loss in the metal contacts [64,157,225]. With rear side reflectance as high as 95%, these structures could bring up to 2.9 mA/cm^2 increase in J_{SC}. In a similar work by Shameli, a polarization independent phase gradient metasurface showed [226] 83% rear side reflectance in simulation. However, surface recombination at the Si/Al boundary was not addressed, which could potentially negatively impact the cell performance.

Dhawan et al. proposed using transformation optics to design photon management structures on Si surfaces, recognizing that texturing the surface increases recombination and it may not be possible to fully passivate it [227]. They proposed using optically equivalent planar layers with varying refractive indices instead of a nano-structured surface. However, it remains uncertain how to fabricate these precise planar layers with varying refractive indices.

Sun et al. suggested using metallic light-trapping electrodes on the front side of the PV cells, which can significantly decrease shadowing

loss and have potential for use in the front-side metal grids, increasing the active area of the cell [228–230].

Khokhar et al. recently designed a TOPcon cell that incorporated a nanosilicon structure on both sides of the cell [231]. By considering both bulk and surface recombination in their simulation, they were able to achieve a J_{SC} of 43.5 mA/cm^2, a V_{OC} of 0.762 V and an FF of 83%. These results are slightly higher than those of practical TOPcon cells reported in Table 1, suggesting that there is potential for further improvement in the performance of practical TOPcon cells through improved photon management and advancements in processing techniques that can reduce recombination losses.

3.4. Combined analysis of the front and read side photon management structures

In a PV cell, both front and rear side photon management structures are needed in order to harness the full potential of the incident light, and together, they contribute to an increase in the J_{SC} of the cell. However, other factors in the cell architecture like cell thickness and surface passivation also contribute to the J_{SC} value. Particularly, surface passivation can impact J_{SC}, V_{OC}, and FF. Therefore, when we compare the contribution of the photon management structures in terms of J_{SC}, the contribution from the surface passivation needs to be decoupled. It is helpful to discuss the photon management structures of the same cell type altogether in this regard. Fig. 2 presents the performance parameters of various recently made Si PV cells, as well as their corresponding photon management techniques and cell types; the cells have been chosen in such a way that they represent a wide variety of photon management techniques and cell types, helping us evaluate their impacts on cell performance. The maximum attainable V_{OC} and J_{SC} from a c-Si PV cells are shown as dotted lines which help determine how far a particular cell is standing from its optimum performance and point to the possible reasons behind that. Table 1 provides additional information on these cells i.e., cell thickness and FF.

The importance of surface passivation is evident in the unpassivated PV cells represented by the data points U17, U22, and U23, which have nanosilicon structures on the front side and planar rear side. These arrangement provided the J_{SC} between 12–21 mA/cm^2. However, as it was challenging to passivate nanosilicon structures, the poor passivation of the front nanostructures resulted in a high recombination loss and very low efficiency. Additionally, U25 and U26 are Si nanowire-based PV cells with no notable photon management structures and surface passivation which caused low V_{OC}, J_{SC} and FF, and extremely low efficiency.

Many data points represent Al-BSF cells where the BSF layer acts as both a passivation layer and reflector. A variety of structures are employed on the front side, including planar, microsilicon, nanosilicon, and nanodielectric structures for photon management. The highest efficiency Al-BSF cell (A11, 20.1% efficiency) has a microsilicon front structure, providing a J_{SC} of 38.6 mA/cm^2 with a Si thickness of 225 μm. The next highest efficiency Al-BSF cell (A49, 19.8% efficiency) has a J_{SC} of 38.77 mA/cm^2. It is important to note that front-side nanostructures have slightly higher J_{SC} values but slightly lower V_{OC} and FF values in the case of A49, likely due to poor surface passivation of the nanostructures. The lowest efficiency Al-BSF cell (A12, 9.24% efficiency) has a microsilicon front structure, poor performance in terms of V_{OC}, J_{SC}, and FF, indicating high recombination. Additionally, in this cell, the 75 μm thickness was not sufficient for capturing incident photons, contributing to a lower J_{SC}.

PERC cells are currently the dominant PV cells in the global market [63,64]. These cells have passivated front and rear sides, reducing surface recombination and achieving high V_{OC}, J_{SC} and FF values with the same photon management as Al-BSF cells. For instance, P47 achieved 21.2% efficiency with a V_{OC} of 0.627 V, J_{SC} of 39.8 mA/cm^2 and FF of 80.58% using a microsilicon front and planar rear. Structuring the rear side while maintaining good surface passivation improves performance further, as seen in cell P32, which has microsilicon structures on both sides and achieved a V_{OC} of 0.684 V, J_{SC} of 39.8 mA/cm^2, FF of 81.54%, and efficiency of 22.61%

The TOPcon cell [83] is a new type of PV cell that significantly reduces surface recombination by utilizing a thin tunneling oxide to passivate the contact, keeping the contact resistivity of the cell almost unchanged. In one of these cells (T55), nanosilicon front side and planar rear provided 41.1 mA/cm^2 J_{SC}, pointing to a good photon management arrangement. This cell achieved a V_{OC} of 0.674 V and an efficiency of 22.3%. However, it was found that the surface passivation of the nanosilicon structure in T55 was not sufficient, prompting the introduction of a new nanosilicon structure in T56 that reduces the difficulty of passivation. This new structure, which involves forming a random pyramid texture and then creating nanoscale pores through reactive ion etching, resulted in increased photocurrent density, V_{OC} and efficiency compared to T55. Another TOPcon cell, T57, used a microsilicon structure on both sides, but did not achieve as high photocurrent density as T55 and T56 due to its relatively higher front reflectance. However, the passivation quality of the microsilicon structure was better, resulting in a higher V_{OC} and efficiency. These examples demonstrate that increasing the photogenerated current does not always improve cell performance and a comprehensive analysis should be conducted when implementing a photon management approach.

The heterojunction cells in the dataset have achieved relatively higher efficiency by using microsilicon structures on both the front and rear sides. This high performance was achieved due to effective photon management, selecting the appropriate cell thickness, and proper surface passivation. For example, H4 demonstrated a V_{OC} of 0.738 V, a photocurrent density of 40.8 mA/cm2, and a FF of 83.36%, resulting in an efficiency of 25.1%. Its performance was surpassed by H2, which achieved an efficiency of 25.6% by using a heterojunction-IBC structure. H2 had a V_{OC} and FF that were similar to H4, but the main improvement came from an increase in photocurrent density (41.8 mA/cm^2) due to the adoption of an IBC structure on the rear side which also trapped some light to the cell.

While it is common to have a textured front and a planar rear side in solar cells, there are also cases where the opposite is used. For instance, the cell IFC28 had a planar front side and a photonic crystal back reflector with a grating structure on the rear side. This arrangement resulted in a photocurrent density of 27.5 mA/cm^2. The V_{OC} and FF of this cell were 0.62 V and 77.42%, respectively. However, the photocurrent density could have been further improved if the front side also had a photon management scheme. Additionally, the cell thickness was 675 μm, a value much greater than the diffusion length [232,233] of silicon (100–300 μm) [97,234,235]. This resulted in some nonradiative recombinations, the absence of which could have led to even higher V_{OC}, J_{SC}, and FF.

A number of cells were investigated with nanodielectric structures on the front side, which provided some level of light trapping compared to cells with no structure on the front. However, these schemes failed to achieve significant efficiency. For example, GSiH46 achieved a V_{OC} of 0.51 V, a photocurrent density of 28 mA/cm^2, and a FF of 61.62% using a bilayer graphene on the front side and a planar rear side. The front reflectance of the cell was less than 5% for the wavelength range of 520–700 nm and less than 10% for longer wavelengths, indicating that the cell was able to capture a good number of photons, yet failed to achieve high efficiency. There are several reasons for this. Firstly, it used whispering gallery mode [171,172] to confine incident light to the cell. However, in this arrangement, perpendicularly incident light does not see any redirection by the front side, as is usually seen for pyramid textured front surfaces (microsilicon structure) [93,94,236]. Secondly, the cell thickness of only 20 μm was not sufficient for adequate light trapping. Additionally, the lower values of V_{OC} and FF also indicate that the surface passivation quality was poor.

4. Practical limit of photon management and improvement pathways

Quantifying the contribution of each technique is crucial in the pursuit of the most effective photon management approach. According to the discussions in the previous section, microsilicon and nanosilicon structures showed the greatest potential for use as front-side photon management structures. Furthermore, when rear side structures such as microsilicon are used, they reflect incident light at an angle which enhances path length further. To determine the highest achievable photocurrent density practically in these configurations, we conducted a study using SunSolve [237]. Pyramid structures were used as a representative of microsilicon structures and black silicon was used as a representative of nanosilicon structures for the front side. On the rear side, both metallic and dielectric rear sides with and without full scattering properties were investigated. Additionally, the impact of cell thickness in the presence of front and rear side photon management mechanisms was also studied (raw data of the study: [238]).

Fig. 4(a) illustrates the performance of different front side photon management structures with a fixed rear side consisting of 1 μm Al-Si + 10 nm Al_2O_3 + 100 nm SiN_X, with no scattering (similar to the rear side structure in Fig. 3(b): metal reflector with dielectric). The cell thickness chosen for this study was 175 μm, a value consistent with the thickness observed in an industrial Si PV cell. The study considers three different front structures: a planar surface, a random pyramid texture, and black Si (5 μm tall, 87.5° sidewall angle), both with and without 75 nm SiN_X on them; SiN_X worked as an ARC. The first part of Fig. 4(a) shows the 1-R (total absorption) and EQE characteristics, where R is the total reflectance of the cell. It is important to note that 1-R accounts for both the absorption in the active region (desired) and the parasitic absorption loss in the front and rear side of the cell (undesired) [57,95]. We observed that a PV cell with a planar silicon surface and no ARC on the front side was able to absorb approximately 60% of the incident light in the 600–1000 nm wavelength range, with a decrease in absorption for other wavelengths. A slight difference between the EQE and 1-R was noticed in the shorter (<400 nm) and longer (> 1100 nm) wavelength ranges, which can be attributed to the parasitic optical absorption on the front and rear sides of the cell respectively. The addition of a 75 nm SiN_X ARC on the planar front side significantly improved the 1-R and EQE of the cell. Additionally, incorporating pyramid textures on the front side also greatly improved the 1-R and EQE compared to a planar surface without an ARC, but exhibited a lower performance in the 430–820 nm range. The highest EQE and 1-R values were achieved using a black silicon front, which was able to absorb approximately 95% of the incident light. Notably, applying an ARC on the black silicon surface resulted in a slight decrease in EQE in the shorter wavelength range, due to parasitic absorption within the ARC. The bar chart in Fig. 4(a) breaks down the total incident light energy into various components [57] including photogenerated current density (J_{SC}), loss in current density due to front reflectance (J_{R-f}) and escape reflectance (J_{R-esc}), and loss in current density due to parasitic optical loss on both the front (J_{loss-f}) and rear sides (J_{loss-r}) of the cell. It indicates that the use of an ARC on planar silicon increased current density by 9 mA/cm^2, primarily as a result of reduced front reflectance loss, however it also slightly increased the escape reflectance loss. This is due to the Si-SiN_X-air boundary having a lower refractive index contrast than the Si-air boundary, making it easier for light to escape. Using a pyramid silicon surface with an ARC structure further reduced both front and escape reflectance loss. However, using a black silicon structure decreased front reflectance loss and parasitic optical loss on both the front and rear sides of the cell, but increased escape reflectance loss. To further reduce escape reflectance loss, the thickness of the cell could be increased until it reaches the minority carrier diffusion length of silicon, allowing for absorption of longer wavelength photons.

We examined the characteristics of various rear-side photon management structures, all of which had the same front structure consisting of a 75 nm SiN_X ARC on a pyramid texture, with a wafer thickness of 175 μm. The structures evaluated included planar Al, Al structures designed to scatter light, planar nickel (Ni, a lossy metal with good electrical transport properties), Ni structures designed to scatter light, planar Al_2O_3 (which has poor electrical transport properties but excellent surface passivation), and Al_2O_3 structures designed to scatter light. Fig. 4(b) indicates that all these rear structures displayed similar EQE and reflectance characteristics in the shorter wavelength range, which can be attributed to their consistent front side structure. However, the rear structure primarily influenced the absorption of the longer wavelength photons. The scattering structures generally exhibited higher absorption than their planar counterparts, as more of the unabsorbed light is reflected back and forth between the front and rear sides, increasing the total path length for absorption in silicon. Additionally, the highest absorption in the longer wavelength range was observed with the Ni structure designed to scatter light, followed by the planar Ni. However, these structures also exhibited the lowest EQE, indicating that most of the absorption occurred in Ni (undesired), rather than silicon. The highest EQE in the longer wavelength range was observed in the case of the Al_2O_3 structure designed to scatter light, due to the absence of parasitic optical loss on the rear side, which is typically present in metals [64,145,146,239]. The bar chart presented in Fig. 4(b) supports the findings that Al_2O_3 structures did not exhibit any J_{loss-r}, while Ni structures exhibited the highest J_{loss-r}. Two key conclusions can be drawn from this information. Firstly, the J_{SC} achieved using the scattering Al_2O_3 structure was 40 mA/cm^2. In order to increase the J_{SC} further with the same front structure, the cell thickness can be increased, doing so however could lead to increased recombination losses in the bulk. Secondly, Al_2O_3 is a dielectric material, using which on the entire rear surface is not allowed as it hinders current collection. A viable solution in this context could involve employing passivating contacts, similar to those used in the TOPCon, HIT or Poly-Si contact architecture.

The impact of the cell thickness on the cell optical performance is illustrated in Fig. 4(c). The cell front side is assumed to be black Si without an ARC and the rear side is assumed to be composed of 1 μm Al-Si, 10 nm Al_2O_3, and 100 nm SiN_X with full scattering. As shorter wavelength photons are absorbed in the front side and are not affected by the cell thickness, we presented the 1-R and EQE characteristics only in the 800–1200 nm wavelength range. As expected, an increase in thickness was observed to increase the 1-R and EQE, but the rate of increase slowed down with increasing thickness.

In light of the findings discussed above, the dataset presented in this paper (Table 1) was analyzed in more detail. The highest efficiency cell had an efficiency of 26.8%, which was achieved using a microsilicon front, and microsilicon rear side. To enhance its light trapping further, a nanostructured front and micro-structured rear with scattering capabilities could potentially be used. However, passivating a nanostructured surface still remains as a significant challenge. Fortunately, there have been some recent advancements in passivating black Si [240–244] which could potentially be utilized in order to improve the performance of the cell further.

5. Conclusion

To minimize the gap between practical efficiency and the Shockley–Queisser limit, it is imperative to incorporate better photon management structures. These structures should exhibit minimal reflectance on the front and high reflectance with scattering properties on the rear side. It is crucial to prevent any contribution to surface recombination or resistive losses. This review comprehensively analyzes various photon management structures, considering V_{OC}, J_{SC}, FF, and efficiency. Many cells underperformed due to the lack of an optimal combination of front and rear structures and inadequate surface passivation. To enhance photon management, it is essential to select an appropriate cell thickness, employ front-side photonic nanostructures reflecting no light

across the solar spectrum, implement rear-side structures with near-perfect reflectance and scattering characteristics in longer wavelengths, and ensure effective passivation of both surfaces. Achieving these goals requires careful consideration of cell architecture, material choices, and process technologies.

CRediT authorship contribution statement

Mohammad Jobayer Hossain: Writing – review & editing, Writing – original draft, Methodology, Investigation, Formal analysis, Conceptualization. **Mengdi Sun:** Writing – original draft, Methodology, Conceptualization. **Kristopher O. Davis:** Writing – review & editing, Supervision, Project administration, Methodology.

Declaration of competing interest

The authors declare that they have no known competing financial interests or personal relationships that could have appeared to influence the work reported in this paper.

Data availability

Datasets related to this article can be found at https://doi.org/10.6084/m9.figshare.23573409.v1, an open source online data repository hosted at figshare [238].

Acknowledgments

This material is based upon work supported by the U.S. Department of Energy's Office of Energy Efficiency and Renewable Energy (EERE) under the Solar Energy Technologies Office, USA Agreement Number DE-EE0007533. The authors would like to acknowledge Prof. Pieter G. Kik for his insightful discussions and valuable perspectives that significantly enhanced the quality of this work. During the preparation of this work, the authors used ChatGPT in order to correct grammatical errors in some parts of the manuscript. After using this tool/service, the authors reviewed and edited the content as needed and take full responsibility for the content of the publication.

References

[1] J. Ellsmoor, Renewable energy is now the cheapest option - even without subsidies, 2019, Forbes Magazine, URL https://www.forbes.com/sites/jamesellsmoor/2019/06/15/renewable-energy-is-now-the-cheapest-option-even-without-subsidies/#4ac481f35a6b.

[2] S. Philipps, W. Warmuth, Photovoltaics Report, Fraunhofer Institute for Solar Energy Systems, ISE, 2020, URL https://www.ise.fraunhofer.de/content/dam/ise/de/documents/publications/studies/Photovoltaics-Report.pdf.

[3] Photovoltaic degradation rates—an analytical review, 21, 2011, http://dx.doi.org/10.1002/pip.1182, URL https://onlinelibrary.wiley.com/doi/abs/10.1002/pip.1182.

[4] K.O. Davis, S.R. Kurtz, D.C. Jordan, J.H. Wohlgemuth, N. Sorloaica-Hickman, Multi-pronged analysis of degradation rates of photovoltaic modules and arrays deployed in florida, Prog. Photovolt., Res. Appl. 21 (4) (2013) 702–712, http://dx.doi.org/10.1002/pip.2154, URL http://onlinelibrary.wiley.com/doi/10.1002/pip.2154/abstract.

[5] D.C. Jordan, S.R. Kurtz, K. VanSant, J. Newmiller, Compendium of photovoltaic degradation rates, Prog. Photovolt., Res. Appl. 24 (7) (2016) 978–989, http://dx.doi.org/10.1002/pip.2744.

[6] D.C. Jordan, B. Marion, C. Deline, T. Barnes, M. Bolinger, PV field reliability status—Analysis of 100 000 solar systems, Prog. Photovolt., Res. Appl. 28 (8) (2020) 739–754, http://dx.doi.org/10.1002/pip.3262, URL http://onlinelibrary.wiley.com/doi/abs/10.1002/pip.3262.

[7] R.H. French, B.D. Huey, A. Longacre, M. Martin, T. Moran, O.V. Kolosov, E. Schneller, A.J. Curran, M. Wang, J. Dai, L.S. Bruckman, J.-N. Jaubert, K.O. Davis, J.L. Braid, M.J. Hossain, R. Frota, N. Iqbal, D.J. Colvin, F. Li, G. Tamizhmani, J.S. Fada, T.D. Wager, X. Ma, J. Sun, J. Liu, A. Pradhan, S. Qin, E.L. Anderson, S.M. Morrison, M.S. Sazally, C.B. Jones, S. Lindig, D. Moser, B. Brownell, C. Whitaker, T.L. Burleyson, A. Khalilnejad, M. Herz, B. Muller, G. Makrides, M. Richter, J. Ascencio-Vasquez, M. van Iseghem, M. Meftah, D.C. Jordan, C. Deline, W. van Sark, J.S. Stein, M. Theristis, B. Meyers, F. Baumgartner, L. Wei, Reliability and Power Degradation Rates of PERC Modules Using Differentiated Packaging Strategies and Characterization Tools, https://doi.org/10.2172/1804123, URL https://www.osti.gov/biblio/1804123.

[8] R. Jones-Albertus, D. Feldman, R. Fu, K. Horowitz, M. Woodhouse, Technology advances needed for photovoltaics to achieve widespread grid price parity, Prog. Photovolt., Res. Appl. 24 (9) (2016) 1272–1283.

[9] At 26.81%, LONGi sets a new world record efficiency for silicon solar cells, URL https://www.longi.com/en/news/propelling-the-transformation/.

[10] Best Research-Cell Efficiency Chart, URL https://www.nrel.gov/pv/assets/pdfs/cell-pv-eff-crysi.pdf.

[11] A. Richter, M. Hermle, S.W. Glunz, Reassessment of the limiting efficiency for crystalline silicon solar cells, IEEE J. Photovolt. 3 (4) (2013) 1184–1191, http://dx.doi.org/10.1109/JPHOTOV.2013.2270351.

[12] S. Jeong, S. Wang, Y. Cui, Nanoscale photon management in silicon solar cells, J. Vacuum Sci. Technol. A 30 (6) (2012) 060801, http://dx.doi.org/10.1116/1.4759260.

[13] A. Peter Amalathas, M.M. Alkaisi, Nanostructures for light trapping in thin film solar cells, Micromachines 10 (9) (2019) http://dx.doi.org/10.3390/mi10090619, URL https://www.mdpi.com/2072-666X/10/9/619.

[14] V.K. Narasimhan, Y. Cui, Nanostructures for photon management in solar cells, Nanophotonics 2 (3) (2013) 187–210, http://dx.doi.org/10.1515/nanoph-2013-0001.

[15] H.-P. Wang, D.-H. Lien, M.-L. Tsai, C.-A. Lin, H.-C. Chang, K.-Y. Lai, J.-H. He, Photon management in nanostructured solar cells, J. Mater. Chem. C 2 (2014) 3144–3171, http://dx.doi.org/10.1039/C3TC32067G.

[16] R. Saive, Light trapping in thin silicon solar cells: A review on fundamentals and technologies, Prog. Photovolt., Res. Appl. 29 (10) (2021) 1125–1137, http://dx.doi.org/10.1002/pip.3440, arXiv:https://onlinelibrary.wiley.com/doi/pdf/10.1002/pip.3440.

[17] C. Battaglia, A. Cuevas, S. De Wolf, High-efficiency crystalline silicon solar cells: status and perspectives, Energy Environ. Sci. (2016) http://dx.doi.org/10.1039/c5ee03380b.

[18] J. Liu, Y. Yao, S. Xiao, X. Gu, Review of status developments of high-efficiency crystalline silicon solar cells, J. Phys. D: Appl. Phys. 51 (12) (2018) 123001, http://dx.doi.org/10.1088/1361-6463/aaac6d, Publisher: IOP Publishing.

[19] H. Steinkemper, M. Hermle, S.W. Glunz, Comprehensive simulation study of industrially relevant silicon solar cell architectures for an optimal material parameter choice, Prog. Photovolt., Res. Appl. (2016) http://dx.doi.org/10.1002/pip.2790.

[20] R. Jaiswal, M. Martínez-Ramón, T. Busani, Recent advances in silicon solar cell research using data science-based learning, IEEE J. Photovolt. (2022).

[21] E. Vazsonyi, K. De Clercq, R. Einhaus, E. Van Kerschaver, K. Said, J. Poortmans, J. Szlufcik, J. Nijs, Improved anisotropic etching process for industrial texturing of silicon solar cells, Solar Energy Mater. Solar Cells 57 (2) (1999) 179–188.

[22] P. Papet, O. Nichiporuk, A. Kaminski, Y. Rozier, J. Kraiem, J.-F. Lelievre, A. Chaumartin, A. Fave, M. Lemiti, Pyramidal texturing of silicon solar cell with TMAH chemical anisotropic etching, Sol. Energy Mater. Sol. Cells 90 (15) (2006) 2319–2328.

[23] K.R. McIntosh, L.P. Johnson, Recombination at textured silicon surfaces passivated with silicon dioxide, J. Appl. Phys. 105 (12) (2009) 124520.

[24] D.H. Macdonald, A. Cuevas, M.J. Kerr, C. Samundsett, D. Ruby, S. Winderbaum, A. Leo, Texturing industrial multicrystalline silicon solar cells, Sol. Energy 76 (1) (2004) 277–283, http://dx.doi.org/10.1016/j.solener.2003.08.019, URL http://www.sciencedirect.com/science/article/pii/S0038092X03003128.

[25] S.C. Baker-Finch, K.R. McIntosh, M.L. Terry, W. Yimao, Isotextured silicon solar cell analysis and modeling 2: Recombination and device modeling, IEEE J. Photovolt. 2 (2012) 465–472, http://dx.doi.org/10.1109/JPHOTOV.2012.2204390.

[26] S.C. Baker-Finch, K.R. McIntosh, M.L. Terry, Isotextured silicon solar cell analysis and modeling 1: Optics, Photovolt. IEEE J. 2 (2012) 457–464, http://dx.doi.org/10.1109/JPHOTOV.2012.2206569.

[27] K. Sreejith, A.K. Sharma, P.K. Basu, A. Kottantharayil, Etching methods for texturing industrial multi-crystalline silicon wafers: A comprehensive review, Sol. Energy Mater. Sol. Cells 238 (2022) 111531, http://dx.doi.org/10.1016/j.solmat.2021.111531, URL https://www.sciencedirect.com/science/article/pii/S0927024821005675.

[28] B. Vermang, A. Rothschild, K. Kenis, K. Wostyn, T. Bearda, A. Racz, X. Loozen, J. John, P.W. Mertens, J. Poortmans, et al., Surface passivation for si solar cells: a combination of advanced surface cleaning and thermal atomic layer deposition of al2o3, in: Solid State Phenomena, Vol. 187, Trans Tech Publ, 2012, pp. 357–361.

[29] A. Moldovan, K. Birmann, J. Rentsch, M. Zimmer, T. Gitte, J. Fittkau, Combined ozone/HF/HCI based cleaning and adjusted emitter etch-back for silicon solar cells, Solid State Phenom. 195 (2013) 305–309, http://dx.doi.org/10.4028/www.scientific.net/SSP.195.305.

[30] I. Kuzma-Filipek, M. Recaman-Payo, M. Aleman, J. John, M. Haslinger, E. Cornagliotti, F. Duerinckx, A. Hajjiah, M. Soha, R. Russel, A. Sharma, A. Uruena, J. Szlufcik, I. Gordon, Simplified cleaning for 22.5% nPERT solar cells with rear epitaxial emitters, Sol. Energy Mater. Sol. Cells (2016) http://dx.doi.org/10.1016/j.solmat.2016.06.036.

[31] H. Ali, A. Moldovan, S. Mack, M. Wilson, W.V. Schoenfeld, K.O. Davis, Influence of surface preparation and cleaning on the passivation of boron diffused silicon surfaces for high efficiency photovoltaics, Thin Solid Films 636 (2017) 412–418, http://dx.doi.org/10.1016/j.tsf.2017.06.043.

[32] A.B. Morales-Vilches, E.-C. Wang, T. Henschel, M. Kubicki, A. Cruz, S. Janke, L. Korte, R. Schlatmann, B. Stannowski, Improved surface passivation by wet texturing, ozone-based cleaning, and plasma-enhanced chemical vapor deposition processes for high-efficiency silicon heterojunction solar cells, Phys. Status Solidi (a) 217 (4) (2020) 1900518, http://dx.doi.org/10.1002/pssa.201900518, URL https://onlinelibrary.wiley.com/doi/abs/10.1002/pssa.201900518.

[33] A. Moldovan, F. Feldmann, G. Krugel, M. Zimmer, J. Rentsch, M. Hermle, A. Roth-Fölsch, K. Kaufmann, C. Hagendorf, Simple cleaning and conditioning of silicon surfaces with UV/ozone sources, Energy Procedia 55 (2014) 834–844.

[34] S. Bakhshi, N. Zin, H. Ali, M. Wilson, D. Chanda, K.O. Davis, W.V. Schoenfeld, Simple and versatile UV-ozone oxide for silicon solar cell applications, Sol. Energy Mater. Sol. Cells 185 (2018) 505–510.

[35] M.Z. Rahman, Advances in surface passivation and emitter optimization techniques of c-si solar cells, Renew. Sustain. Energy Rev. 30 (2014) 734–742, http://dx.doi.org/10.1016/j.rser.2013.11.025.

[36] H. Hieslmair, L. Mandrell, I. Latchford, M. Chun, J. Sullivan, B. Adibi, High throughput ion-implantation for silicon solar cells, Energy Procedia 27 (2012) 122–128.

[37] A. Rohatgi, D.L. Meier, B. McPherson, Y.-W. Ok, A.D. Upadhyaya, J.-H. Lai, F. Zimbardi, High-throughput ion-implantation for low-cost high-efficiency silicon solar cells, Energy Procedia 15 (2012) 10–19.

[38] K.O. Davis, K. Jiang, C. Demberger, H. Zunft, H. Haverkamp, D. Habermann, W.V. Schoenfeld, Improved control of the phosphorous surface concentration during in-line diffusion of c-si solar cells by APCVD, Phys. Status Solidi (RRL) 7 (5) (2013) 319–321.

[39] P. Rothhardt, C. Demberger, A. Wolf, D. Biro, Co-diffusion from APCVD BSG and POCl3 for industrial n-type solar cells, Energy Procedia 38 (2013) 305–311.

[40] H. Wagner, A. Dastgheib-Shirazi, B. Min, A.E. Morishige, M. Steyer, G. Hahn, C. del Cañizo, T. Buonassisi, P.P. Altermatt, Optimizing phosphorus diffusion for photovoltaic applications: Peak doping, inactive phosphorus, gettering, and contact formation, J. Appl. Phys. 119 (18) (2016) 185704.

[41] A.G. Aberle, Overview on sin surface passivation of crystalline silicon solar cells, Sol. Energy Mater. Sol. Cells 65 (2001) 239–248, http://dx.doi.org/10.1016/S0927-0248(00)00099-4.

[42] A.G. Aberle, Surface passivation of crystalline silicon solar cells: A review, Prog. Photovolt., Res. Appl. 8 (2000) 473–487, http://dx.doi.org/10.1002/1099-159X(200009/10)8:5<473::AID-PIP337>3.0.CO;2-D.

[43] A. Cuevas, Y. Wan, D. Yan, C. Samundsett, T. Allen, X. Zhang, J. Cui, J. Bullock, Carrier population control and surface passivation in solar cells, Sol. Energy Mater. Sol. Cells 184 (2018) 38–47, http://dx.doi.org/10.1016/j.solmat.2018.04.026, URL http://www.sciencedirect.com/science/article/pii/S0927024818302010.

[44] G. Dingemans, W.M.M. Kessels, Status and prospects of al2o3-based surface passivation schemes for silicon solar cells, J. Vacuum Sci. Technol. A 30 (2012) 040802–1–040802–27, http://dx.doi.org/10.1116/1.4728205.

[45] M. Rahman, S. Khan, Advances in surface passivation of c-si solar cells, Mater. Renew. Sustain. Energy 1 (2012) 1–11, http://dx.doi.org/10.1007/s40243-012-0001-y.

[46] R.S. Bonilla, B. Hoex, P. Hamer, P.R. Wilshaw, Dielectric surface passivation for silicon solar cells: A review: Dielectric surface passivation for silicon solar cells, Phys. Status Solidi (a) 214 (7) (2017) 1700293, http://dx.doi.org/10.1002/pssa.201700293, URL http://doi.wiley.com/10.1002/pssa.201700293.

[47] C. Ballif, D. Huljić, G. Willeke, A. Hessler-Wyser, Silver thick-film contacts on highly doped n-type silicon emitters: structural and electronic properties of the interface, Appl. Phys. Lett. 82 (12) (2003) 1878–1880.

[48] G. Schubert, F. Huster, P. Fath, Physical understanding of printed thick-film front contacts of crystalline si solar cells—Review of existing models and recent developments, Solar Energy Mater. Solar Cells 90 (18–19) (2006) 3399–3406.

[49] A. Ebong, N. Chen, Metallization of crystalline silicon solar cells: A review, in: High Capacity Optical Networks and Emerging/Enabling Technologies, 2012, pp. 102–109, http://dx.doi.org/10.1109/HONET.2012.6421444.

[50] A. Kaminski, B. Vandelle, A. Fave, J.P. Boyeaux, L. Quan Nam, R. Monna, D. Sarti, A. Laugier, Aluminium BSF in silicon solar cells, Sol. Energy Mater. Sol. Cells 72 (2002) 373–379.

[51] J.D. Fields, M.I. Ahmad, V.L. Pool, J. Yu, D.G. Van Campen, P.A. Parilla, M.F. Toney, M.F.A.M. van Hest, The formation mechanism for printed silver-contacts for silicon solar cells, Nature Commun. 7 (2016) 11143, http://dx.doi.org/10.1038/ncomms11143, URL https://www.nature.com/articles/ncomms11143.

[52] V. Shanmugam, J. Wong, I.M. Peters, J. Cunnusamy, M. Zahn, A. Zhou, R. Yang, X. Chen, A.G. Aberle, T. Mueller, Analysis of fine-line screen and stencil-printed metal contacts for silicon wafer solar cells, IEEE J. Photovolt. 5 (2) (2015) 525–533, http://dx.doi.org/10.1109/JPHOTOV.2014.2388073.

[53] J. Zhang, H. Tong, X. Sun, G. Li, H. Li, Y. Yang, X. Yuan, C. Liu, H. Li, An investigation on determinants of silver paste metallization contact performance on crystalline silicon solar cells, J. Mater. Sci., Mater. Electron. (2020) http://dx.doi.org/10.1007/s10854-020-03145-9.

[54] S. Xiong, X. Yuan, Y. Yang, J. Zhang, H. Tong, C. Liu, X. Ye, S. Li, L. Luo, X. Wang, Macroscopic study on current transport path in front-side contacts of crystalline silicon solar cells, Physica Status Solidi (a) 1900480, http://dx.doi.org/10.1002/pssa.201900480, URL https://onlinelibrary.wiley.com/doi/abs/10.1002/pssa.201900480.

[55] S. Tepner, N. Wengenmeyr, M. Linse, A. Lorenz, M. Pospischil, F. Clement, The link between ag-paste rheology and screen-printed solar cell metallization, Adv. Mater. Technol. 5 (10) (2020) 2000654, http://dx.doi.org/10.1002/admt.202000654, URL https://www.onlinelibrary.wiley.com/doi/abs/10.1002/admt.202000654, _eprint: https://onlinelibrary.wiley.com/doi/pdf/10.1002/admt.202000654.

[56] E.J. Schneller, M.J. Hossain, R. Frota, A.J. Curran, M. Wang, J.-N. Jaubert, J.L. Braid, R.H. French, K.O. Davis, Performance evaluation of commercially relevant p-type silicon cell architectures, in: 2019 IEEE 46th Photovoltaic Specialists Conference, PVSC, 2019, pp. 0326–0329, http://dx.doi.org/10.1109/PVSC40753.2019.8980618.

[57] M.J. Hossain, G. Gregory, H. Patel, S. Guo, E.J. Schneller, A.M. Gabor, Z. Yang, A.L. Blum, K.O. Davis, Detailed performance loss analysis of silicon solar cells using high-throughput metrology methods, in: 2018 IEEE 7th World Conference on Photovoltaic Energy Conversion (WCPEC) (a Joint Conference of 45th IEEE PVSC, 28th PVSEC 34th EU PVSEC), 2018, pp. 2214–2218, http://dx.doi.org/10.1109/PVSC.2018.8547869.

[58] A.W. Blakers, A. Wang, A.M. Milne, J. Zhao, M.A. Green, 22.8% Efficient silicon solar cell, Appl. Phys. Lett. 55 (13) (1989) 1363–1365, http://dx.doi.org/10.1063/1.101596.

[59] M.A. Green, A.W. Blakers, J. Zhao, A.M. Milne, A. Wang, X. Dai, Characterization of 23-% efficient silicon solar cells, IEEE Trans. Electron Devices 37 (2) (1990) 331–336.

[60] A. Blakers, Development of the PERC solar cell, IEEE J. Photovolt. 9 (3) (2019) 629–635.

[61] T. Dullweber, J. Schmidt, Industrial silicon solar cells applying the passivated emitter and rear cell (PERC) concept—A review, IEEE J. Photovolt. 6 (5) (2016) 1366–1381, http://dx.doi.org/10.1109/JPHOTOV.2016.2571627.

[62] B. Min, M. Müller, H. Wagner, G. Fischer, R. Brendel, P.P. Altermatt, H. Neuhaus, A roadmap toward 24% efficient PERC solar cells in industrial mass production, IEEE J. Photovolt. 7 (6) (2017) 1541–1550, http://dx.doi.org/10.1109/JPHOTOV.2017.2749007.

[63] R. Preu, E. Lohmüller, S. Lohmüller, P. Saint-Cast, J.M. Greulich, Passivated emitter and rear cell—Devices, technology, and modeling, Appl. Phys. Rev. 7 (4) (2020) 041315, http://dx.doi.org/10.1063/5.0005090.

[64] M.J. Hossain, M. Sun, G. Doerk, P.G. Kik, K.O. Davis, Self-assembled multifunctional nanostructures for surface passivation and photon management in silicon photovoltaics, Nanophotonics 10 (18) (2021) 4611–4621, http://dx.doi.org/10.1515/nanoph-2021-0472.

[65] S.D. Wolf, A. Descoeudres, Z.C. Holman, C. Ballif, High-efficiency silicon heterojunction solar cells: A review, Green 2 (1) (2012) 7–24, http://dx.doi.org/10.1515/green-2011-0018.

[66] A. Razzaq, T.G. Allen, W. Liu, Z. Liu, S. De Wolf, Silicon heterojunction solar cells: Techno-economic assessment and opportunities, Joule 6 (3) (2022) 514–542, http://dx.doi.org/10.1016/j.joule.2022.02.009, URL https://www.sciencedirect.com/science/article/pii/S2542435122000903.

[67] M. Taguchi, Review—Development history of high efficiency silicon heterojunction solar cell: From discovery to practical use, ECS J. Solid State Sci. Technol. 10 (2) (2021) 025002, http://dx.doi.org/10.1149/2162-8777/abdfb6.

[68] A. Louwen, W. van Sark, R. Schropp, A. Faaij, A cost roadmap for silicon heterojunction solar cells, Sol. Energy Mater. Sol. Cells 147 (2016) 295–314, http://dx.doi.org/10.1016/j.solmat.2015.12.026.

[69] J. Haschke, O. Dupré, M. Boccard, C. Ballif, Silicon heterojunction solar cells: Recent technological development and practical aspects - from lab to industry, Sol. Energy Mater. Sol. Cells 187 (2018) 140–153, http://dx.doi.org/10.1016/j.solmat.2018.07.018, URL http://www.sciencedirect.com/science/article/pii/S0927024818303805.

[70] Y. Liu, Y. Li, Y. Wu, G. Yang, L. Mazzarella, P. Procel-Moya, A.C. Tamboli, K. Weber, M. Boccard, O. Isabella, X. Yang, B. Sun, High-efficiency silicon heterojunction solar cells: Materials, devices and applications, Mater. Sci. Eng. R 142 (2020) 100579, http://dx.doi.org/10.1016/j.mser.2020.100579, URL http://www.sciencedirect.com/science/article/pii/S0927796X20300371.

[71] E. Yablonovitch, T. Gmitter, R.M. Swanson, Y.H. Kwark, A 720 mv open circuit voltage siox:c-si:Siox double heterostructure solar cell, Appl. Phys. Lett. 47 (1985) 1211, http://dx.doi.org/10.1063/1.96331.

[72] F. Haase, C. Hollemann, S. Schäfer, A. Merkle, M. Rienäcker, J. Krügener, R. Brendel, R. Peibst, Laser contact openings for local poly-si-metal contacts enabling 26.1%-efficient POLO-IBC solar cells, Sol. Energy Mater. Sol. Cells 186 (2018) 184–193, http://dx.doi.org/10.1016/j.solmat.2018.06.020, URL https://www.sciencedirect.com/science/article/pii/S0927024818303076.

[73] F. Haase, S. Schäfer, C. Klamt, F. Kiefer, J. Krügener, R. Brendel, R. Peibst, Perimeter recombination in 25%-efficient IBC solar cells with passivating POLO contacts for both polarities, IEEE J. Photovolt. 8 (1) (2018) 23–29, http://dx.doi.org/10.1109/JPHOTOV.2017.2762592.

[74] R. Peibst, U. Römer, Y. Larionova, M. Rienäcker, A. Merkle, N. Folchert, S. Reiter, M. Turcu, B. Min, J. Krügener, D. Tetzlaff, E. Bugiel, T. Wietler, R. Brendel, Working principle of carrier selective poly-si/c-si junctions: Is tunnelling the whole story? Sol. Energy Mater. Sol. Cells 158 (2016) 60–67, http://dx.doi.org/10.1016/j.solmat.2016.05.045, URL http://www.sciencedirect.com/science/article/pii/S0927024816301519.

[75] S. Duttagupta, N. Nandakumar, P. Padhamnath, J.K. Buatis, R. Stangl, A.G. Aberle, Monopoly™ cells: Large-area crystalline silicon solar cells with fire-through screen printed contact to doped polysilicon surfaces, Sol. Energy Mater. Sol. Cells 187 (2018) 76–81, http://dx.doi.org/10.1016/j.solmat.2018.05.059, URL http://www.sciencedirect.com/science/article/pii/S092702481830285X.

[76] P. Padhamnath, J. Wong, B. Nagarajan, J.K. Buatis, L.M. Ortega, N. Nandakumar, A. Khanna, V. Shanmugam, S. Duttagupta, Metal contact recombination in monopoly™ solar cells with screen-printed & fire-through contacts, Sol. Energy Mater. Sol. Cells 192 (2019) 109–116, http://dx.doi.org/10.1016/j.solmat.2018.12.026, URL http://www.sciencedirect.com/science/article/pii/S0927024818305919.

[77] F. Feldmann, M. Bivour, C. Reichel, M. Hermle, S.W. Glunz, Passivated rear contacts for high-efficiency n-type si solar cells providing high interface passivation quality and excellent transport characteristics, Sol. Energy Mater. Sol. Cells 120 (2014) 270–274, http://dx.doi.org/10.1016/j.solmat.2013.09.017, URL http://www.sciencedirect.com/science/article/pii/S0927024813004868.

[78] F. Feldmann, M. Bivour, C. Reichel, H. Steinkemper, M. Hermle, S.W. Glunz, Tunnel oxide passivated contacts as an alternative to partial rear contacts, Sol. Energy Mater. Sol. Cells 131 (2014) 46–50, http://dx.doi.org/10.1016/j.solmat.2014.06.015, URL http://www.sciencedirect.com/science/article/pii/S0927024814003249.

[79] Y. Chen, D. Chen, C. Liu, Z. Wang, Y. Zou, Y. He, Y. Wang, L. Yuan, J. Gong, W. Lin, X. Zhang, Y. Yang, H. Shen, Z. Feng, P.P. Altermatt, P.J. Verlinden, Mass production of industrial tunnel oxide passivated contacts (i-TOPCon) silicon solar cells with average efficiency over 23% and modules over 345 W, Prog. Photovolt., Res. Appl. 27 (10) (2019) 827–834, http://dx.doi.org/10.1002/pip.3180, URL https://onlinelibrary.wiley.com/doi/abs/10.1002/pip.3180.

[80] D. Chen, Y. Chen, Z. Wang, J. Gong, C. Liu, Y. Zou, Y. He, Y. Wang, L. Yuan, W. Lin, R. Xia, L. Yin, X. Zhang, G. Xu, Y. Yang, H. Shen, Z. Feng, P.P. Altermatt, P.J. Verlinden, 24.58% Total area efficiency of screen-printed, large area industrial silicon solar cells with the tunnel oxide passivated contacts (i-TOPCon) design, Sol. Energy Mater. Sol. Cells 206 (2020) 110258, http://dx.doi.org/10.1016/j.solmat.2019.110258, URL http://www.sciencedirect.com/science/article/pii/S0927024819305872.

[81] B. Kafle, B.S. Goraya, S. Mack, F. Feldmann, S. Nold, J. Rentsch, TOPCon – technology options for cost efficient industrial manufacturing, Sol. Energy Mater. Sol. Cells 227 (2021) 111100, http://dx.doi.org/10.1016/j.solmat.2021.111100, URL https://www.sciencedirect.com/science/article/pii/S0927024821001422.

[82] D.K. Ghosh, S. Bose, G. Das, S. Acharyya, A. Nandi, S. Mukhopadhyay, A. Sengupta, Fundamentals, present status and future perspective of TOPCon solar cells: A comprehensive review, Surf. Interfaces 30 (2022) 101917, http://dx.doi.org/10.1016/j.surfin.2022.101917, URL https://www.sciencedirect.com/science/article/pii/S2468023022001973.

[83] F. Feldmann, M. Bivour, C. Reichel, M. Hermle, S.W. Glunz, Passivated rear contacts for high-efficiency n-type si solar cells providing high interface passivation quality and excellent transport characteristics, Sol. Energy Mater. Sol. Cells 120 (2014) 270–274, http://dx.doi.org/10.1016/j.solmat.2013.09.017, URL https://www.sciencedirect.com/science/article/pii/S0927024813004868.

[84] J.F. Mousumi, H. Ali, G. Gregory, C. Nunez, K. Provancha, S. Seren, H. Zunft, K.O. Davis, Phosphorus-doped polysilicon passivating contacts deposited by atmospheric pressure chemical vapor deposition, J. Phys. D: Appl. Phys. 54 (38) (2021) 384003, http://dx.doi.org/10.1088/1361-6463/ac0e5c, Publisher: IOP Publishing.

[85] J.F. Mousumi, G. Gregory, J.P. Ganesan, C. Nunez, K. Provancha, S. Seren, H. Zunft, T. Jurca, P. Banerjee, A. Kar, R. Kumar, K.O. Davis, Process–structure–properties relationships of passivating, electron-selective contacts formed by atmospheric pressure chemical vapor deposition of phosphorus-doped polysilicon, Phys. Status Solidi (RRL) 16 (5) (2022) 2100639, http://dx.doi.org/10.1002/pssr.202100639, URL https://onlinelibrary.wiley.com/doi/10.1002/pssr.202100639.

[86] D. Yan, A. Cuevas, J.I. Michel, C. Zhang, Y. Wan, X. Zhang, J. Bullock, Polysilicon passivated junctions: The next technology for silicon solar cells? Joule 5 (4) (2021) 811–828, http://dx.doi.org/10.1016/j.joule.2021.02.013, URL https://www.cell.com/joule/abstract/S2542-4351(21)00090-8, Publisher: Elsevier.

[87] E.V. Kerschaver, G. Beaucarne, Back-contact solar cells: A review, Prog. Photovolt., Res. Appl. 14 (2) (2006) 107–123.

[88] M.M. Desa, S. Sapeai, A. Azhari, K. Sopian, M. Sulaiman, N. Amin, S. Zaidi, Silicon back contact solar cell configuration: A pathway towards higher efficiency, Renew. Sustain. Energy Rev. 60 (2016) 1516–1532.

[89] Q. Pengcheng, Q. Pengxiang, Characteristics and development of interdigital back contact solar cells, IOP Conf. Series: Earth Environ. Sci. 621 (1) (2021) 012067, http://dx.doi.org/10.1088/1755-1315/621/1/012067.

[90] H. Lin, M. Yang, X. Ru, G. Wang, S. Yin, F. Peng, C. Hong, M. Qu, J. Lu, L. Fang, et al., Silicon heterojunction solar cells with up to 26.81 achieved by electrically optimized nanocrystalline-silicon hole contact layers, Nat. Energy 8 (8) (2023) 789–799, http://dx.doi.org/10.1038/s41560-023-01255-2.

[91] C.A. Gueymard, D. Myers, K. Emery, Proposed reference irradiance spectra for solar energy systems testing, Solar Energy 73 (6) (2002) 443–467.

[92] W. Shockley, The theory of p-n junctions in semiconductors and p-n junction transistors, Bell Syst. Tech. J. 28 (3) (1949) 435–489.

[93] D. Kray, M. Hermle, S.W. Glunz, Theory and experiments on the back side reflectance of silicon wafer solar cells, Prog. Photovolt., Res. Appl. 16 (1) (2008) 1–15.

[94] K.O. Davis, K. Jiang, C. Demberger, H. Zunft, H. Haverkamp, D. Habermann, W.V. Schoenfeld, Investigation of the internal back reflectance of rear-side dielectric stacks for c-Si solar cells, IEEE J. Photovolt. 3 (2) (2013) 641–648.

[95] M.J. Hossain, G. Gregory, E.J. Schneller, A.M. Gabor, A.L. Blum, Z. Yang, D. Sulas, S. Johnston, K.O. Davis, A comprehensive methodology to evaluate losses and process variations in silicon solar cell manufacturing, IEEE J. Photovolt. 9 (5) (2019) 1350–1359, http://dx.doi.org/10.1109/JPHOTOV.2019.2926628.

[96] E.J. Schneller, K. Öğütman, S. Guo, W.V. Schoenfeld, K.O. Davis, Crystalline silicon device loss analysis through spatially resolved quantum efficiency measurements, IEEE J. Photovolt. 7 (4) (2017) 957–965.

[97] M.J. Hossain, G. Gregory, E. Schneller, K. Davis, Dataset - a comprehensive methodology to evaluate losses and process variations in silicon solar cell manufacturing, 2019, http://dx.doi.org/10.6084/m9.figshare.7636922.v2, URL https://figshare.com/articles/dataset/Dataset_-_A_Comprehensive_Methodology_to_Evaluate_Losses_and_Process_Variations_in_Silicon_Solar_Cell_Manufacturing/7636922/2.

[98] M.J. Hossain, E.J. Schneller, M. Li, K.O. Davis, Incorporation of spatially-resolved current density measurements with photoluminescence for advanced parameter imaging of solar cells, Sol. Energy Mater. Sol. Cells 199 (2019) 136–143.

[99] E.J. Schneller, M.J. Hossain, R. Frota, N. Iqbal, D. Colvin, A.J. Curran, M. Wang, J.L. Braid, L.S. Bruckman, R.H. French, B.D. Huey, J.N. Jaubert, K.O. Davis, Spatially resolved characterization of optical and recombination losses for different industrial silicon solar cell architectures, Internat. J. Modern Phys. B 34 (21) (2020) http://dx.doi.org/10.1142/S0217979220502045, 2050204–3.

[100] M.J. Kerr, A. Cuevas, R.A. Sinton, Generalized analysis of quasi-steady-state and transient decay open circuit voltage measurements, J. Appl. Phys. 91 (2002) 399, http://dx.doi.org/10.1063/1.1416134.

[101] R.A. Sinton, A. Cuevas, Contactless determination of current–voltage characteristics and minority carrier lifetimes in semiconductors from quasi-steady-state photoconductance data, Appl. Phys. Lett. 69 (1996) 2510–2512.

[102] M. Bivour, J. Temmler, H. Steinkemper, M. Hermle, Molybdenum and tungsten oxide: High work function wide band gap contact materials for hole selective contacts of silicon solar cells, Sol. Energy Mater. Sol. Cells 142 (2015) 34–41, http://dx.doi.org/10.1016/j.solmat.2015.05.031.

[103] L. Neusel, M. Bivour, M. Hermle, Selectivity issues of moox based hole contacts, Energy Procedia 124 (2017) 425–434, http://dx.doi.org/10.1016/j.egypro.2017.09.268, URL http://www.sciencedirect.com/science/article/pii/S1876610217341991.

[104] J. Melskens, B.W.H.v. Loo, B. Macco, L.E. Black, S. Smit, W.M.M. Kessels, Passivating contacts for crystalline silicon solar cells: From concepts and materials to prospects, IEEE J. Photovolt. 8 (2) (2018) 373–388, http://dx.doi.org/10.1109/JPHOTOV.2018.2797106.

[105] A. Onno, C. Chen, P. Koswatta, M. Boccard, Z.C. Holman, Passivation, conductivity, and selectivity in solar cell contacts: Concepts and simulations based on a unified partial-resistances framework, J. Appl. Phys. 126 (18) (2019) 183103, http://dx.doi.org/10.1063/1.5117201, URL https://aip.scitation.org/doi/full/10.1063/1.5117201, Publisher: American Institute of Physics.

[106] U. Rau, T. Kirchartz, Charge carrier collection and contact selectivity in solar cells, Adv. Mater. Interfaces 6 (20) (2019) 1900252, http://dx.doi.org/10.1002/admi.201900252, Publisher: John Wiley & Sons, Ltd.

[107] L. Serenelli, L. Martini, F. Menchini, M. Izzi, G.d. Cesare, G. Condorelli, C. Gerardi, D. Muñoz, M. Tucci, Selective contacts and fill factor limitations in heterojunction solar cells, Prog. Photovolt., Res. Appl. 29 (7) (2021) 876–884, http://dx.doi.org/10.1002/pip.3418, URL https://onlinelibrary.wiley.com/doi/abs/10.1002/pip.3418, _eprint: https://onlinelibrary.wiley.com/doi/pdf/10.1002/pip.3418.

[108] M. Leilaeioun, Z.C. Holman, Accuracy of expressions for the fill factor of a solar cell in terms of open-circuit voltage and ideality factor, J. Appl. Phys. 120 (12) (2016).

[109] B. Richards, Single-material TiO2 double-layer antireflection coatings, Sol. Energy Mater. Sol. Cells 79 (3) (2003) 369–390.

[110] J. Kim, J. Park, J.H. Hong, S.J. Choi, G.H. Kang, G.J. Yu, N.S. Kim, H.-e. Song, Double antireflection coating layer with silicon nitride and silicon oxide for crystalline silicon solar cell, J. Electroceram. 30 (2013) 41–45.

[111] K.O. Davis, K. Jiang, D. Habermann, W.V. Schoenfeld, Tailoring the optical properties of APCVD titanium oxide films for all-oxide multilayer antireflection coatings, IEEE J. Photovolt. 5 (5) (2015) 1265–1270.

[112] D.-S. Wuu, C.-C. Lin, C.-N. Chen, H.-H. Lee, J.-J. Huang, Properties of double-layer Al2O3/TiO2 antireflection coatings by liquid phase deposition, Thin Solid Films 584 (2015) 248–252.

[113] R.S. Bonilla, K.O. Davis, E.J. Schneller, W.V. Schoenfeld, P.R. Wilshaw, Effective antireflection and surface passivation of silicon using a SiO2/a-TiOx film stack, IEEE J. Photovolt. 7 (6) (2017) 1603–1610, http://dx.doi.org/10.1109/JPHOTOV.2017.2753198.

[114] X. Yan, N. Chen, F.B. Suhaimi, L. Zhang, X. Gong, X. Zhang, S. Duttagupta, Design, fabrication, and analysis of double-layer antireflection coatings (ARC) for industrial bifacial n-type crystalline silicon solar cells, Appl. Opt. 58 (15) (2019) E1–E6.

[115] Z.C. Holman, A. Descoeudres, L. Barraud, F.Z. Fernandez, J.P. Seif, S. De Wolf, C. Ballif, Current losses at the front of silicon heterojunction solar cells, IEEE J. Photovolt. 2 (1) (2012) 7–15.

[116] C. Battaglia, X. Yin, M. Zheng, I.D. Sharp, T. Chen, S. McDonnell, A. Azcatl, C. Carraro, B. Ma, R. Maboudian, R.M. Wallace, A. Javey, Hole selective moox contact for silicon solar cells, Nano Lett. 14 (2014) 967–971, http://dx.doi.org/10.1021/nl404389u.

[117] C. Battaglia, S.M. de Nicolás, S. De Wolf, X. Yin, M. Zheng, C. Ballif, A. Javey, Silicon heterojunction solar cell with passivated hole selective MoOx contact, Appl. Phys. Lett. 104 (2014) 113902, http://dx.doi.org/10.1063/1.4868880.

[118] J. Bullock, A. Cuevas, T. Allen, C. Battaglia, Molybdenum oxide MoOx: A versatile hole contact for silicon solar cells, Appl. Phys. Lett. 105 (2014) 232109, http://dx.doi.org/10.1063/1.4903467.

[119] B. Macco, M.F.J. Vos, N.F.W. Thissen, A.A. Bol, W.M.M. Kessels, Low-temperature atomic layer deposition of moox for silicon heterojunction solar cells, Phys. Status Solidi (RRL) 9 (7) (2015) 393–396, http://dx.doi.org/10.1002/pssr.201510117, URL http://onlinelibrary.wiley.com/doi/abs/10.1002/pssr.201510117, _eprint: https://onlinelibrary.wiley.com/doi/pdf/10.1002/pssr.201510117.

[120] J. Bullock, M. Hettick, J. Geissbühler, A.J. Ong, T. Allen, C.M. Sutter-Fella, T. Chen, H. Ota, E.W. Schaler, S. De Wolf, C. Ballif, A. Cuevas, A. Javey, Efficient silicon solar cells with dopant-free asymmetric heterocontacts, Nat. Energy 1 (3) (2016) 15031, http://dx.doi.org/10.1038/nenergy.2015.31.

[121] X. Yang, Q. Bi, H. Ali, K.O. Davis, W.V. Schoenfeld, K. Weber, High performance TiO2-based electron-selective contacts for crystalline silicon solar cells, Adv. Mater. 28 (2016) 5891–5897, http://dx.doi.org/10.1002/adma.201600926.

[122] L.G. Gerling, C. Voz, R. Alcubilla, J. Puigdollers, Origin of passivation in hole-selective transition metal oxides for crystalline silicon heterojunction solar cells, J. Mater. Res. 32 (2) (2017) 260–268, http://dx.doi.org/10.1557/jmr.2016.453, Publisher: Cambridge University Press.

[123] T.G. Allen, J. Bullock, Q. Jeangros, C. Samundsett, Y. Wan, J. Cui, A. Hessler-Wyser, S. De Wolf, A. Javey, A. Cuevas, A low resistance calcium/reduced titania passivated contact for high efficiency crystalline silicon solar cells, Adv. Energy Mater. 7 (12) (2017) 1602606, http://dx.doi.org/10.1002/aenm.201602606, URL http://onlinelibrary.wiley.com/doi/10.1002/aenm.201602606/abstract.

[124] T. Matsui, M. Bivour, P. Ndione, P. Hettich, M. Hermle, Investigation of atomic-layer-deposited tiox as selective electron and hole contacts to crystalline silicon, Energy Procedia 124 (2017) 628–634, http://dx.doi.org/10.1016/j.egypro.2017.09.093, URL http://www.sciencedirect.com/science/article/pii/S1876610217339371.

[125] Y. Wan, C. Samundsett, J. Bullock, M. Hettick, T. Allen, D. Yan, J. Peng, Y. Wu, J. Cui, A. Javey, A. Cuevas, Conductive and stable magnesium oxide electron-selective contacts for efficient silicon solar cells, Adv. Energy Mater. 7 (5) (2017) 1601863, http://dx.doi.org/10.1002/aenm.201601863, URL https://onlinelibrary.wiley.com/doi/abs/10.1002/aenm.201601863, _eprint: https://onlinelibrary.wiley.com/doi/pdf/10.1002/aenm.201601863.

[126] Y. Wan, S.K. Karuturi, C. Samundsett, J. Bullock, M. Hettick, D. Yan, J. Peng, P.R. Narangari, S. Mokkapati, H.H. Tan, C. Jagadish, A. Javey, A. Cuevas, Tantalum oxide electron-selective heterocontacts for silicon photovoltaics and photoelectrochemical water reduction, ACS Energy Lett. 3 (1) (2018) 125–131, http://dx.doi.org/10.1021/acsenergylett.7b01153.

[127] H. Ali, S. Koul, G. Gregory, J. Bullock, A. Javey, A. Kushima, K.O. Davis, Thermal stability of hole-selective tungsten oxide: In situ transmission electron microscopy study, Sci. Rep. 8 (1) (2018) 12651, http://dx.doi.org/10.1038/s41598-018-31053-w, URL https://www.nature.com/articles/s41598-018-31053-w.

[128] B. Macco, L.E. Black, J. Melskens, B.W.H. van de Loo, W.-J.H. Berghuis, M.A. Verheijen, W.M.M. Kessels, Atomic-layer deposited Nb2O5 as transparent passivating electron contact for c-Si solar cells, Sol. Energy Mater. Sol. Cells 184 (2018) 98–104, http://dx.doi.org/10.1016/j.solmat.2018.04.037, URL http://www.sciencedirect.com/science/article/pii/S0927024818302125.

[129] H. Ali, S. Koul, G. Gregory, J. Bullock, A. Javey, A. Kushima, K.O. Davis, In situ transmission electron microscopy study of molybdenum oxide contacts for silicon solar cells, Phys. Status Solidi (a) 216 (7) (2019) 1800998, http://dx.doi.org/10.1002/pssa.201800998, URL https://onlinelibrary.wiley.com/doi/abs/10.1002/pssa.201800998.

[130] B.E. Davis, N.C. Strandwitz, Aluminum oxide passivating tunneling interlayers for molybdenum oxide hole-selective contacts, IEEE J. Photovolt. (2020) 1–7, http://dx.doi.org/10.1109/JPHOTOV.2020.2973447, Conference Name: IEEE Journal of Photovoltaics.

[131] T. Matsui, M. Bivour, P.F. Ndione, R.S. Bonilla, M. Hermle, Origin of the tunable carrier selectivity of atomic-layer-deposited tiox nanolayers in crystalline silicon solar cells, Sol. Energy Mater. Sol. Cells 209 (2020) 110461, http://dx.doi.org/10.1016/j.solmat.2020.110461, URL http://www.sciencedirect.com/science/article/pii/S0927024820300672.

[132] J. Dréon, Q. Jeangros, J. Cattin, J. Haschke, L. Antognini, C. Ballif, M. Boccard, 23.5%-Efficient silicon heterojunction silicon solar cell using molybdenum oxide as hole-selective contact, Nano Energy (2020) 104495, http://dx.doi.org/10.1016/j.nanoen.2020.104495, URL http://www.sciencedirect.com/science/article/pii/S2211285520300525.

[133] G. Gregory, C. Feit, Z. Gao, P. Banerjee, T. Jurca, K.O. Davis, Improving the passivation of molybdenum oxide hole-selective contacts with 1 nm hydrogenated aluminum oxide films for silicon solar cells, Phys. Status Solidi (a) 217 (15) (2020) 2000093, http://dx.doi.org/10.1002/pssa.202000093, URL http://onlinelibrary.wiley.com/doi/abs/10.1002/pssa.202000093, _eprint: https://onlinelibrary.wiley.com/doi/pdf/10.1002/pssa.202000093.

[134] K. Öğütman, N. Iqbal, G. Gregory, M. Li, M. Haslinger, E. Cornagliotti, W.V. Schoenfeld, J. John, K.O. Davis, Spatial atomic layer deposition of aluminum oxide as a passivating hole contact for silicon solar cells, Phys. Status Solidi (a) 217 (18) (2020) 2000348, http://dx.doi.org/10.1002/pssa.202000348, URL http://onlinelibrary.wiley.com/doi/abs/10.1002/pssa.202000348, _eprint: https://onlinelibrary.wiley.com/doi/pdf/10.1002/pssa.202000348.

[135] G. Gregory, C. Luderer, H. Ali, T.S. Sakthivel, T. Jurca, M. Bivour, S. Seal, K.O. Davis, Spatial atomic layer deposition of molybdenum oxide for industrial solar cells, Adv. Mater. Interfaces 7 (22) (2020) 2000895, http://dx.doi.org/10.1002/admi.202000895, URL http://onlinelibrary.wiley.com/doi/abs/10.1002/admi.202000895, _eprint: https://onlinelibrary.wiley.com/doi/pdf/10.1002/admi.202000895.

[136] X. Yang, H. Xu, W. Liu, Q. Bi, L. Xu, J. Kang, M.N. Hedhili, B. Sun, X. Zhang, S.D. Wolf, Atomic layer deposition of vanadium oxide as hole-selective contact for crystalline silicon solar cells, Adv. Electr. Mater. n/a (n/a) 2000467, http://dx.doi.org/10.1002/aelm.202000467, URL http://onlinelibrary.wiley.com/doi/abs/10.1002/aelm.202000467, _eprint: https://onlinelibrary.wiley.com/doi/pdf/10.1002/aelm.202000467.

[137] T. Fellmeth, A. Born, A. Kimmerle, F. Clement, D. Biro, R. Preu, Recombination at metal-emitter interfaces of front contact technologies for highly efficient silicon solar cells, Energy Procedia 8 (2011) 115–121, http://dx.doi.org/10.1016/j.egypro.2011.06.111, URL http://www.sciencedirect.com/science/article/pii/S1876610211016201.

[138] V. Shanmugam, T. Mueller, A.G. Aberle, J. Wong, Determination of metal contact recombination parameters for silicon wafer solar cells by photoluminescence imaging, Sol. Energy 118 (2015) 20–27, http://dx.doi.org/10.1016/j.solener.2015.05.010.

[139] M. Li, J. Wong, N. Chen, A.G. Aberle, R. Stangl, Determination of metallization-induced recombination losses of screen-printed silicon solar cell contacts and their dependence on the doping profile, IEEE J. Photovolt. 8 (6) (2018) 1470–1477, http://dx.doi.org/10.1109/JPHOTOV.2018.2866177, URL https://ieeexplore.ieee.org/document/8454790/.

[140] R. Dumbrell, M.K. Juhl, T. Trupke, Z. Hameiri, Extracting metal contact recombination parameters from effective lifetime data, IEEE J. Photovolt. 8 (6) (2018) 1413–1420.

[141] M. Li, N. Iqbal, Z. Yang, X. Lin, N.K. Pannaci, C. Avalos, T. Shaw, T. Jurca, K. Davis, A comprehensive evaluation of contact recombination and contact resistivity losses in industrial silicon solar cells, IEEE J. Photovolt. 10 (5) (2020) 1277–1282, http://dx.doi.org/10.1109/JPHOTOV.2020.3003792, Conference Name: IEEE Journal of Photovoltaics.

[142] D. Herrmann, D.R. Falconi, S. Lohmüller, D. Ourinson, A. Fell, H. Höffler, A.A. Brand, A. Wolf, Spatially resolved determination of metallization-induced recombination losses using photoluminescence imaging, IEEE J. Photovolt. 11 (1) (2020) 174–184.

[143] S. Guo, G. Gregory, A.M. Gabor, W.V. Schoenfeld, K.O. Davis, Detailed investigation of TLM contact resistance measurements on crystalline silicon solar cells, Sol. Energy 151 (2017) 163–172.

[144] G. Gregory, M. Li, A. Gabor, A. Anselmo, Z. Yang, H. Ali, N. Iqbal, K. Davis, Nondestructive contact resistivity measurements on solar cells using the circular transmission line method, IEEE J. Photovolt. 9 (6) (2019) 1800–1805, http://dx.doi.org/10.1109/JPHOTOV.2019.2945173.

[145] Z.C. Holman, M. Filipič, B. Lipovšek, S. De Wolf, F. Smole, M. Topič, C. Ballif, Parasitic absorption in the rear reflector of a silicon solar cell: Simulation and measurement of the sub-bandgap reflectance for common dielectric/metal reflectors, Sol. Energy Mater. Sol. Cells 120 (2014) 426–430, http://dx.doi.org/10.1016/j.solmat.2013.06.024, URL https://www.sciencedirect.com/science/article/pii/S0927024813003097.

[146] Z.C. Holman, M. Filipič, A. Descoeudres, S. De Wolf, F. Smole, M. Topič, C. Ballif, Infrared light management in high-efficiency silicon heterojunction and rear-passivated solar cells, J. Appl. Phys. 113 (1) (2013) 013107, http://dx.doi.org/10.1063/1.4772975.

[147] M. Otto, M. Kroll, T. Käsebier, R. Salzer, A. Tünnermann, R.B. Wehrspohn, Extremely low surface recombination velocities in black silicon passivated by atomic layer deposition, Appl. Phys. Lett. 100 (19) (2012).

[148] P. Repo, A. Haarahiltunen, L. Sainiemi, M. Yli-Koski, H. Talvitie, M.C. Schubert, H. Savin, Effective passivation of black silicon surfaces by atomic layer deposition, IEEE J. Photovolt. 3 (1) (2012) 90–94.

[149] W.-C. Wang, C.-W. Lin, H.-J. Chen, C.-W. Chang, J.-J. Huang, M.-J. Yang, B. Tjahjono, J.-J. Huang, W.-C. Hsu, M.-J. Chen, Surface passivation of efficient nanotextured black silicon solar cells using thermal atomic layer deposition, ACS Appl. Mater. Interfaces 5 (19) (2013) 9752–9759.

[150] P. Repo, J. Benick, G.v. Gastrow, V. Vähänissi, F.D. Heinz, J. Schön, M.C. Schubert, H. Savin, Passivation of black silicon boron emitters with atomic layer deposited aluminum oxide, Phys. Status Solidi (RRL) 7 (11) (2013) 950–954.

[151] M. Algasinger, J. Paye, F. Werner, J. Schmidt, M.S. Brandt, M. Stutzmann, S. Koynov, Improved black silicon for photovoltaic applications, Adv. Energy Mater. 3 (8) (2013) 1068–1074.

[152] G. Von Gastrow, R. Alcubilla, P. Ortega, M. Yli-Koski, S. Conesa-Boj, A.F. i Morral, H. Savin, Analysis of the atomic layer deposited al2o3 field-effect passivation in black silicon, Sol. Energy Mater. Sol. Cells 142 (2015) 29–33.

[153] B. Van De Loo, A. Ingenito, M. Verheijen, O. Isabella, M. Zeman, W. Kessels, Surface passivation of n-type doped black silicon by atomic-layer-deposited SiO2/Al2O3 stacks, Appl. Phys. Lett. 110 (26) (2017).

[154] T. Rahman, R.S. Bonilla, A. Nawabjan, P.R. Wilshaw, S.A. Boden, Passivation of all-angle black surfaces for silicon solar cells, Sol. Energy Mater. Sol. Cells 160 (2017) 444–453, http://dx.doi.org/10.1016/j.solmat.2016.10.044, URL http://www.sciencedirect.com/science/article/pii/S0927024816304652.

[155] F. Ji, C. Zhou, J. Zhu, W. Wang, Improvement of the surface structure for the surface passivation of black silicon, IEEE J. Photovolt. 10 (4) (2020) 978–985.

[156] S. Wang, X. Wu, F.-J. Ma, D. Payne, M. Abbott, B. Hoex, Field-effect passivation of undiffused black silicon surfaces, IEEE J. Photovolt. 11 (4) (2021) 897–907.

[157] M.J. Hossain, Measurement and mitigation of optical, recombination and resistive losses in silicon photovoltaics, Electron. Theses Diss. (2021) URL https://stars.library.ucf.edu/etd2020/1495.

[158] B. Vermang, H. Goverde, A. Uruena, A. Lorenz, E. Cornagliotti, A. Rothschild, J. John, J. Poortmans, R. Mertens, Blistering in ALD Al2o3 passivation layers as rear contacting for local Al BSF Si solar cells, Sol. Energy Mater. Sol. Cells 101 (2012) 204–209, http://dx.doi.org/10.1016/j.solmat.2012.01.032, URL http://www.sciencedirect.com/science/article/pii/S0927024812000487.

[159] A. Volk, N. Tucher, J. Seiffe, H. Hauser, M. Zimmer, B. Bläsi, M. Hofmann, J. Rentsch, Honeycomb structure on multi-crystalline silicon Al-BSF solar cell with 17.8% efficiency, IEEE J. Photovolt. 5 (4) (2015) 1027–1033, http://dx.doi.org/10.1109/JPHOTOV.2015.2402757.

[160] H.-P. Wang, J.-H. He, Toward highly efficient nanostructured solar cells using concurrent electrical and optical design, Adv. Energy Mater. 7 (23) 1602385, http://dx.doi.org/10.1002/aenm.201602385, arXiv:https://onlinelibrary.wiley.com/doi/pdf/10.1002/aenm.201602385.

[161] S. Jeong, M.D. McGehee, Y. Cui, All-back-contact ultra-thin silicon nanocone solar cells with 13.7% power conversion efficiency, Nature Commun. 4 (2950) (2013) http://dx.doi.org/10.1038/ncomms3950.

[162] A. Cordaro, S.W. Tabernig, M. Pollard, C. Yi, E. Alarcon-Llado, B. Hoex, A. Polman, Nanopatterned SiN x broadband antireflection coating for planar silicon solar cells, Phys. Status Solidi (a) 220 (5) (2023) 2200827, http://dx.doi.org/10.1002/pssa.202200827, arXiv:https://onlinelibrary.wiley.com/doi/pdf/10.1002/pssa.202200827.

[163] K. Lee, I. Hwang, N. Kim, D. Choi, H.-D. Um, S. Kim, K. Seo, 17.6% Efficient radial junction solar cells using silicon nano/micro hybrid structures, Nanoscale 8 (2016) 14473–14479, http://dx.doi.org/10.1039/C6NR04611H.

[164] B. Kafle, A. Mannan, T. Freund, L. Clochard, E. Duffy, M. Hofmann, J. Rentsch, R. Preu, Nanotextured multicrystalline al-BSF solar cells reaching 18% conversion efficiency using industrially viable solar cell processes, Phys. Status Solidi (RRL) 9 (8) (2015) 448–452, http://dx.doi.org/10.1002/pssr.201510219, arXiv:https://onlinelibrary.wiley.com/doi/pdf/10.1002/pssr.201510219.

[165] T. Fellmeth, S. Mack, J. Bartsch, D. Erath, U. Jäger, R. Preu, F. Clement, D. Biro, 20.1% Efficient silicon solar cell with aluminum back surface field, IEEE Electron Device Lett. 32 (8) (2011) 1101–1103, http://dx.doi.org/10.1109/LED.2011.2157656.

[166] H. Savin, P. Repo, G. von Gastrow, P. von Gastrow, E. Calle, M. Garín, R. Alcubilla, Black silicon solar cells with interdigitated back-contacts achieve 22.1% efficiency, Nature Nanotechnol. 10 (2015) 624–628, http://dx.doi.org/10.1038/nnano.2015.89.

[167] M. Garín, T.P. Pasanen, G. López, V. Vähänissi, K. Chen, I. Martín, H. Savin, Black ultra-thin crystalline silicon wafers reach the 4n2 absorption limit–application to IBC solar cells, Small 19 (39) (2023) 2302250, http://dx.doi.org/10.1002/smll.202302250, arXiv:https://onlinelibrary.wiley.com/doi/pdf/10.1002/smll.202302250.

[168] J. Xu, C. Chen, C. Liu, J. Chen, Z. Liu, X. Yuan, H. Li, High efficiency topcon solar cells with micron/nano-structured emitter for a balance of light-trapping and surface passivation, Sol. Energy Mater. Sol. Cells 238 (2022) 111606, http://dx.doi.org/10.1016/j.solmat.2022.111606, URL https://www.sciencedirect.com/science/article/pii/S0927024822000307.

[169] S.V. Boriskina, T.A. Cooper, L. Zeng, G. Ni, J.K. Tong, Y. Tsurimaki, Y. Huang, L. Meroueh, G. Mahan, G. Chen, Losses in plasmonics: from mitigating energy dissipation to embracing loss-enabled functionalities, Adv. Opt. Photon. 9 (4) (2017) 775–827, http://dx.doi.org/10.1364/AOP.9.000775, URL https://opg.optica.org/aop/abstract.cfm?URI=aop-9-4-775.

[170] Y. Yao, J. Yao, V.K. Narasimhan, Z. Ruan, C. Xie, S. Fan, Y. Cui, Broadband light management using low-q whispering gallery modes in spherical nanoshells, Nature Commun. 3 (664) (2012) http://dx.doi.org/10.1038/ncomms1664.

[171] J. Grandidier, D.M. Callahan, J.N. Munday, H.A. Atwater, Light absorption enhancement in thin-film solar cells using whispering gallery modes in dielectric nanospheres, Adv. Mater. 23 (10) (2011) 1272–1276, http://dx.doi.org/10.1002/adma.201004393, arXiv:https://onlinelibrary.wiley.com/doi/pdf/10.1002/adma.201004393.

[172] Y. Yao, J. Yao, V.K. Narasimhan, Z. Ruan, C. Xie, S. Fan, Y. Cui, Broadband light management using low-q whispering gallery modes in spherical nanoshells., Nat. Commun. 3 (2012) 664, http://dx.doi.org/10.1038/ncomms1664.

[173] K. Yoshikawa, H. Kawasaki, W. Yoshida, T. Irie, K. Konishi, K. Nakano, T. Uto, D. Adachi, M. Kanematsu, H. Uzu, K. Yamamoto, Silicon heterojunction solar cell with interdigitated back contacts for a photoconversion efficiency over 26%, Nat. Energy 2 (17032) (2017) http://dx.doi.org/10.1038/nenergy.2017.32.

[174] K. Masuko, M. Shigematsu, T. Hashiguchi, D. Fujishima, M. Kai, N. Yoshimura, T. Yamaguchi, Y. Ichihashi, T. Mishima, N. Matsubara, T. Yamanishi, T. Takahama, M. Taguchi, E. Maruyama, S. Okamoto, Achievement of more than 25% conversion efficiency with crystalline silicon heterojunction solar cell, IEEE J. Photovolt. 4 (6) (2014) 1433–1435, http://dx.doi.org/10.1109/JPHOTOV.2014.2352151.

[175] D.D. Smith, G. Reich, M. Baldrias, M. Reich, N. Boitnott, G. Bunea, Silicon solar cells with total area efficiency above 25%, in: 2016 IEEE 43rd Photovoltaic Specialists Conference, PVSC, 2016, pp. 3351–3355, http://dx.doi.org/10.1109/PVSC.2016.7750287.

[176] D. Adachi, J. Hernández, K. Yamamoto, Impact of carrier recombination on fill factor for large area heterojunction crystalline silicon solar cell with 25.1% efficiency, Appl. Phys. Lett. 107 (23) (2015) 233506, http://dx.doi.org/10.1063/1.4937224.

[177] M. Taguchi, A. Yano, S. Tohoda, K. Matsuyama, Y. Nakamura, T. Nishiwaki, K. Fujita, E. Maruyama, 24.7% Record efficiency HIT solar cell on thin silicon wafer, IEEE J. Photovolt. 4 (1) (2014) 96–99, http://dx.doi.org/10.1109/JPHOTOV.2013.2282737.

[178] X. Li, J. Li, T. Chen, B. Tay, J. Wang, H. Yu, Periodically aligned si nanopillar arrays as efficient antireflection layers for solar cell applications, Nanoscale Res. Lett. 5 (1721) (2010) http://dx.doi.org/10.1007/s11671-010-9701-3.

[179] W.-C. Tu, Y.-T. Chang, H.-P. Wang, C.-H. Yang, C.-T. Huang, J.-H. He, S.-C. Lee, Improved light scattering and surface plasmon tuning in amorphous silicon solar cells by double-walled carbon nanotubes, Sol. Energy Mater. Sol. Cells 101 (2012) 200–203, http://dx.doi.org/10.1016/j.solmat.2012.01.038, URL http://www.sciencedirect.com/science/article/pii/S0927024812000542.

[180] D. Yang, F. Lang, Z. Xu, J. Shi, G. Li, Z. Hu, J. Xiong, Influence of atomic layer deposition al2o3nano-layer on the surface passivation of silicon solar cells, J. Semicond. 35 (5) (2014) 052002, http://dx.doi.org/10.1088/1674-4926/35/5/052002.

[181] C. Lin, K. Lai, W. Lien, J. He, An efficient broadband and omnidirectional light-harvesting scheme employing a hierarchical structure based on a ZnO nanorod/Si3N4-coated si microgroove on 5-inch single crystalline si solar cells, Nanoscale (2012) http://dx.doi.org/10.1039/C2NR32358C.

[182] J.-Y. Jung, Z. Guo, S.-W. Jee, H.-D. Um, K.-T. Park, M.S. Hyun, J.M. Yang, J.-H. Lee, A waferscale si wire solar cell using radial and bulk p–n junctions, Nanotechnology 21 (44) (2010) 445303, http://dx.doi.org/10.1088/0957-4484/21/44/445303.

[183] K.-Q. Peng, X. Wang, L. Li, X.-L. Wu, S.-T. Lee, High-performance silicon nanohole solar cells, J. Am. Chem. Soc. 132 (20) (2010) 6872–6873, http://dx.doi.org/10.1021/ja910082y, PMID: 20426468.

[184] E. Garnett, P. Yang, Light trapping in silicon nanowire solar cells, Nano Lett. 10 (3) (2010) 1082–1087, http://dx.doi.org/10.1021/nl100161z, PMID: 20108969.

[185] B. Tian, X. Zheng, T. Kempa, Y. Fang, N. Yu, G. Yu, J. Huang, C. Lieber, Coaxial silicon nanowires as solar cells and nanoelectronic power sources, Nature 449 (2007) 885–889, http://dx.doi.org/10.1038/nature06181.

[186] T.J. Kempa, B. Tian, D.R. Kim, J. Hu, X. Zheng, C.M. Lieber, Single and tandem axial p-i-n nanowire photovoltaic devices, Nano Lett. 8 (10) (2008) 3456–3460, http://dx.doi.org/10.1021/nl8023438, PMID: 18763836.

[187] E.C. Garnett, P. Yang, Silicon nanowire radial pn junction solar cells, J. Am. Chem. Soc. 130 (29) (2008) 9224–9225, http://dx.doi.org/10.1021/ja8032907, PMID: 18576622.

[188] J. Zhu, C.-M. Hsu, Z. Yu, S. Fan, Y. Cui, Nanodome solar cells with efficient light management and self-cleaning, Nano Lett. 10 (6) (2010) 1979–1984, http://dx.doi.org/10.1021/nl9034237, PMID: 19891462.

[189] L. Zeng, Y. Yi, C. Hong, J. Liu, N. Feng, X. Duan, L.C. Kimerling, B.A. Alamariu, Efficiency enhancement in si solar cells by textured photonic crystal back reflector, Appl. Phys. Lett. 89 (11) (2006) 111111, http://dx.doi.org/10.1063/1.2349845.

[190] I. Kuzma-Filipek, K. Nieuwenhuysen, J. Hoeymissen, M. Payo, E. Kerschaver, J. Poortmans, R. Mertens, G. Beaucarne, E. Schmich, S. Lindekugel, S. Reber, Efficiency (>15%) for thin-film epitaxial silicon solar cells on 70cm2 area offspec silicon substrate using porous silicon segmented mirrors, Prog. Photovolt., Res. Appl. 18 (2) (2010) 137–143, http://dx.doi.org/10.1002/pip.953, arXiv:https://onlinelibrary.wiley.com/doi/pdf/10.1002/pip.953.

[191] H. Hannebauer, T. Dullweber, U. Baumann, T. Falcon, R. Brendel, 21.2% Efficient fineline-printed PERC solar cell with 5 busbar front grid, Phys. Status Solidi (RRL) 8 (8) (2014) 675–679, http://dx.doi.org/10.1002/pssr.201409190, arXiv:https://onlinelibrary.wiley.com/doi/pdf/10.1002/pssr.201409190.

[192] H. Huang, J. Lv, Y. Bao, R. Xuan, S. Sun, S. Sneck, S. Li, C. Modanese, H. Savin, A. Wang, J. Zhao, 20.8% Industrial PERC solar cell: ALD Al2O3 rear surface passivation, efficiency loss mechanisms analysis and roadmap to 24%, Sol. Energy Mater. Sol. Cells 161 (2017) 14–30, http://dx.doi.org/10.1016/j.solmat.2016.11.018, URL http://www.sciencedirect.com/science/article/pii/S0927024816304901.

[193] W. Deng, F. Ye, R. Liu, Y. Li, H. Chen, Z. Xiong, Y. Yang, Y. Chen, Y. Wang, P.P. Altermatt, Z. Feng, P.J. Verlinden, 22.61% Efficient fully screen printed PERC solar cell, in: 2017 IEEE 44th Photovoltaic Specialist Conference, PVSC, 2017, pp. 2220–2226, http://dx.doi.org/10.1109/PVSC.2017.8366416.

[194] M. Xue, K.N. Nazif, Z. Lyu, J. Jiang, C.-Y. Lu, N. Lee, K. Zang, Y. Chen, T. Zheng, T.I. Kamins, M.L. Brongersma, K.C. Saraswat, J.S. Harris, Free-standing 2.7 μ m thick ultrathin crystalline silicon solar cell with efficiency above 12.0%, Nano Energy 70 (2020) 104466, http://dx.doi.org/10.1016/j.nanoen.2020.104466, URL https://www.sciencedirect.com/science/article/pii/S2211285520300227.

[195] R. Chen, H. Tong, H. Zhu, C. Ding, H. Li, D. Chen, B. Hallam, C.M. Chong, S. Wenham, A. Ciesla, 23.83% Efficient mono-PERC incorporating advanced hydrogenation, Prog. Photovolt., Res. Appl. 28 (12) (2020) 1239–1247, http://dx.doi.org/10.1002/pip.3243, arXiv:https://onlinelibrary.wiley.com/doi/pdf/10.1002/pip.3243.

[196] C. Hollemann, F. Haase, S. Schäfer, J. Krügener, R. Brendel, R. Peibst, 26.1%-Efficient POLO-IBC cells: Quantification of electrical and optical loss mechanisms, Prog. Photovolt., Res. Appl. 27 (11) (2019) 950–958, http://dx.doi.org/10.1002/pip.3098, arXiv:https://onlinelibrary.wiley.com/doi/pdf/10.1002/pip.3098.

[197] M.S. Branham, W.-C. Hsu, S. Yerci, J. Loomis, S.V. Boriskina, B.R. Hoard, S.E. Han, G. Chen, 15.7% Efficient 10-μ m-thick crystalline silicon solar cells using periodic nanostructures, Adv. Mater. 27 (13) (2015) 2182–2188, http://dx.doi.org/10.1002/adma.201405511, arXiv:https://onlinelibrary.wiley.com/doi/pdf/10.1002/adma.201405511.

[198] J.H. Petermann, D. Zielke, J. Schmidt, F. Haase, E.G. Rojas, R. Brendel, 19%-Efficient and 43 μ m-thick crystalline si solar cell from layer transfer using porous silicon, Prog. Photovolt., Res. Appl. 20 (1) (2012) 1–5, http://dx.doi.org/10.1002/pip.1129, arXiv:https://onlinelibrary.wiley.com/doi/pdf/10.1002/pip.1129.

[199] W. Wang, J. He, D. Yan, C. Samundsett, S.P. Phang, Z. Huang, W. Shen, J. Bullock, Y. Wan, 21.3%-Efficient n-type silicon solar cell with a full area rear TiOx/LiF/Al electron-selective contact, Sol. Energy Mater. Sol. Cells 206 (2020) 110291, http://dx.doi.org/10.1016/j.solmat.2019.110291, URL https://www.sciencedirect.com/science/article/pii/S0927024819306208.

[200] J. Cho, N. Nawal, A. Hadipour, M. Recaman Payo, A. van der Heide, H.S. Radhakrishnan, M. Debucquoy, I. Gordon, J. Szlufcik, J. Poortmans, Interface analysis and intrinsic thermal stability of MoOx based hole-selective contacts for silicon heterojunction solar cells, Sol. Energy Mater. Sol. Cells 201 (2019) 110074, http://dx.doi.org/10.1016/j.solmat.2019.110074, URL https://www.sciencedirect.com/science/article/pii/S0927024819304039.

[201] X. Yang, E. Aydin, H. Xu, J. Kang, M. Hedhili, W. Liu, Y. Wan, J. Peng, C. Samundsett, A. Cuevas, S. De Wolf, Tantalum nitride electron-selective contact for crystalline silicon solar cells, Adv. Energy Mater. 8 (20) (2018) 1800608, http://dx.doi.org/10.1002/aenm.201800608, arXiv:https://onlinelibrary.wiley.com/doi/pdf/10.1002/aenm.201800608.

[202] A. Descoeudres, C. Allebé, N. Badel, L. Barraud, J. Champliaud, G. Christmann, F. Debrot, A. Faes, J. Geissbühler, J. Horzel, A. Lachowicz, J. Levrat, S. Martin de Nicolas, S. Nicolay, B. Paviet-Salomon, L.-L. Senaud, C. Ballif, M. Despeisse, Low-temperature processes for passivation and metallization of high-efficiency crystalline silicon solar cells, Sol. Energy 175 (2018) 54–59, http://dx.doi.org/10.1016/j.solener.2018.01.074, URL https://www.sciencedirect.com/science/article/pii/S0038092X18300951, Recent Progress in Photovoltaics, Part 1.

[203] T.G. Allen, J. Bullock, Q. Jeangros, C. Samundsett, Y. Wan, J. Cui, A. Hessler-Wyser, S. De Wolf, A. Javey, A. Cuevas, A low resistance calcium/reduced titania passivated contact for high efficiency crystalline silicon solar cells, Adv. Energy Mater. 7 (12) (2017) 1602606, http://dx.doi.org/10.1002/aenm.201602606, arXiv:https://onlinelibrary.wiley.com/doi/pdf/10.1002/aenm.201602606.

[204] X. Yang, Q. Bi, H. Ali, K. Davis, W.V. Schoenfeld, K. Weber, High-performance TiO2-based electron-selective contacts for crystalline silicon solar cells, Adv. Mater. 28 (28) (2016) 5891–5897, http://dx.doi.org/10.1002/adma.201600926, arXiv:https://onlinelibrary.wiley.com/doi/pdf/10.1002/adma.201600926.

[205] S. Das, M.J. Hossain, S.-F. Leung, A. Lenox, Y. Jung, K. Davis, J.-H. He, T. Roy, A leaf-inspired photon management scheme using optically tuned bilayer nanoparticles for ultra-thin and highly efficient photovoltaic devices, Nano Energy 58 (2019) 47–56, http://dx.doi.org/10.1016/j.nanoen.2018.12.072, URL https://www.sciencedirect.com/science/article/pii/S2211285518309856.

[206] F.-I. Lai, J.-F. Yang, Y.-C. Hsu, S.-Y. Kuo, Enhanced conversion efficiency of a-Si:H thin-film solar cell using ZnO nanorods, Crystals 10 (12) (2020) http://dx.doi.org/10.3390/cryst10121082, URL https://www.mdpi.com/2073-4352/10/12/1082.

[207] Y. Lee, Y. Woo, D.-K. Lee, I. Kim, Fabrication of quasi-hexagonal si nanostructures and its application for flexible crystalline ultrathin si solar cells, Sol. Energy 208 (2020) 957–965, http://dx.doi.org/10.1016/j.solener.2020.08.063, URL https://www.sciencedirect.com/science/article/pii/S0038092X20309026.

[208] Q. Tang, H. Yao, B. Xu, J. Ge, Enhanced energy conversion efficiency of Al-BSF c-Si solar cell by a novel hierarchical structure composed of inverted pyramids with different sizes, Sol. Energy 208 (2020) 1–9, http://dx.doi.org/10.1016/j.solener.2020.07.073, URL https://www.sciencedirect.com/science/article/pii/S0038092X20308057.

[209] C. Huang, K. Sun, W.-L. Chang, Efficiency enhancement of silicon solar cells using a nano-scale honeycomb broadband anti-reflection structure, Opt. Express 20 (S1) (2012) A85–A93, http://dx.doi.org/10.1364/OE.20.000A85, URL http://www.opticsexpress.org/abstract.cfm?URI=oe-20-101-A85.

[210] X. Yu, D. Wang, D. Lei, Efficiency improvement of silicon solar cells enabled by ZnO nanowhisker array coating, Nanoscale Res. Lett. 7 (306) (2012) http://dx.doi.org/10.1186/1556-276X-7-306.

[211] Y. Jiang, H. Shen, T. Pu, C. Zheng, Q. Tang, K. Gao, J. Wu, C. Rui, Y. Li, Y. Liu, High efficiency multi-crystalline silicon solar cell with inverted pyramid nanostructure, Sol. Energy 142 (2017) 91–96, http://dx.doi.org/10.1016/j.solener.2016.12.007, URL https://www.sciencedirect.com/science/article/pii/S0038092X16306041.

[212] S. Kim, J. Park, P.D. Phong, C. Shin, S.M. Iftiquar, J. Yi, Improving the efficiency of rear emitter silicon solar cell using an optimized n-type silicon oxide front surface field layer, Sci. Rep. 8 (2018) http://dx.doi.org/10.1038/s41598-018-28823-x.

[213] L. Yang, Y. Liu, Y. Wang, W. Chen, Q. Chen, J. Wu, A. Kuznetsov, X. Du, 18.87%-Efficient inverted pyramid structured silicon solar cell by one-step cu-assisted texturization technique, Sol. Energy Mater. Sol. Cells 166 (2017) 121–126, http://dx.doi.org/10.1016/j.solmat.2017.03.017, URL https://www.sciencedirect.com/science/article/pii/S0927024817301307.

[214] F. Schindler, A. Fell, R. Müller, J. Benick, A. Richter, F. Feldmann, P. Krenckel, S. Riepe, M.C. Schubert, S.W. Glunz, Towards the efficiency limits of multicrystalline silicon solar cells, Sol. Energy Mater. Sol. Cells 185 (2018) 198–204, http://dx.doi.org/10.1016/j.solmat.2018.05.006, URL https://www.sciencedirect.com/science/article/pii/S0927024818302186.

[215] D. Chen, Y. Chen, Z. Wang, J. Gong, C. Liu, Y. Zou, Y. He, Y. Wang, L. Yuan, W. Lin, R. Xia, L. Yin, X. Zhang, G. Xu, Y. Yang, H. Shen, Z. Feng, P.P. Altermatt, P.J. Verlinden, 24.58 Silicon solar cells with the tunnel oxide passivated contacts (i-topcon) design, Sol. Energy Mater. Sol. Cells 206 (2020) 110258, http://dx.doi.org/10.1016/j.solmat.2019.110258, URL https://www.sciencedirect.com/science/article/pii/S0927024819305872.

[216] M.A. Green, The path to 25% silicon solar cell efficiency: History of silicon cell evolution, Prog. Photovolt., Res. Appl. 17 (3) (2009) 183–189, http://dx.doi.org/10.1002/pip.892, arXiv:https://onlinelibrary.wiley.com/doi/pdf/10.1002/pip.892.

[217] K. Münzera, J. Schöne, A. Teppe, M. Hein, R. Schlosser, M. Hanke, K. Varner, H. Mäckel, S. Keller, P. Fath, Physical properties of industrial 19 solar cells, Energy Procedia 8 (2011) 415–420, http://dx.doi.org/10.1016/j.egypro.2011.06.159, URL https://www.sciencedirect.com/science/article/pii/S1876610211016687, Proceedings of the SiliconPV 2011 Conference (1st International Conference on Crystalline Silicon Photovoltaics).

[218] H. Hannebauer, T. Dullweber, U. Baumann, T. Falcon, R. Brendel, 21.2% Efficient fineline-printed PERC solar cell with 5 busbar front grid, Phys. Status Solidi (RRL) 8 (8) (2014) 675–679, http://dx.doi.org/10.1002/pssr.201409190, arXiv:https://onlinelibrary.wiley.com/doi/pdf/10.1002/pssr.201409190.

[219] A. Cordaro, R. Müller, S.W. Tabernig, N. Tucher, P. Schygulla, O. Höhn, B. Bläsi, A. Polman, Nanopatterned back-reflector with engineered near-field/far-field light scattering for enhanced light trapping in silicon-based multijunction solar cells, ACS Photonics (2023) 4061–4070.

[220] H. Heidarzadeh, A. Rostami, M. Dolatyari, G. Rostami, Plasmon-enhanced performance of an ultrathin silicon solar cell using metal-semiconductor core-shell hemispherical nanoparticles and metallic back grating, Appl. Opt. 55 (7) (2016) 1779–1785, http://dx.doi.org/10.1364/AO.55.001779, URL http://opg.optica.org/ao/abstract.cfm?URI=ao-55-7-1779.

[221] F. Zhao, J. Lin, Z. Lei, Z. Yi, F. Qin, J. Zhang, L. Liu, X. Wu, W. Yang, P. Wu, Realization of 18.97% theoretical efficiency of 0.9 μ m thick c-Si/ZnO heterojunction ultrathin-film solar cells via surface plasmon resonance enhancement, Phys. Chem. Chem. Phys. 24 (2022) 4871–4880, http://dx.doi.org/10.1039/D1CP05119A.

[222] M. Wang, H. He, C. Shou, H. Cui, D. Yang, L. Wang, Anti-reflection effect of large-area ZnO nano-needle array on multi-crystalline silicon solar cells, Mater. Sci. Semicond. Process. 138 (2022) 106299, http://dx.doi.org/10.1016/j.mssp.2021.106299, URL https://www.sciencedirect.com/science/article/pii/S1369800121006338.

[223] J. Zhu, D. Hu, Y. Wang, C. Tao, H. Jia, W. Zhao, Efficient light trapping from nanorod-like single-textured al-doped ZnO transparent conducting films, Coatings 11 (5) (2021) URL https://www.mdpi.com/2079-6412/11/5/513.

[224] S. Saravanan, R. Dubey, Performance enhancement of amorphous silicon solar cell using 1d photonic crystal as back reflector, Mater. Today: Proc. 49 (2022) 2822–2825, http://dx.doi.org/10.1016/j.matpr.2021.09.536, URL https://www.sciencedirect.com/science/article/pii/S2214785321064701, Indo-UK International Virtual Conference on Advanced Nanomaterials for Energy and Environmental Applications (ICANEE-2020).

[225] M.J. Hossain, N. Iqbal, G. Doerk, K.O. Davis, Enhanced light trapping in carrier selective solar cells using photonic nanostructures, in: B. Panchapakesan, A.-J. Attias (Eds.), Nanoengineering: Fabrication, Properties, Optics, Thin Films, and Devices XVI, Vol. 11089, International Society for Optics and Photonics, SPIE, 2019, p. 110890P, http://dx.doi.org/10.1117/12.2528984.

[226] M.A. Shameli, P. Salami, L. Yousefi, Light trapping in thin film solar cells using a polarization independent phase gradient metasurface, J. Opt. 20 (12) (2018) 125004, http://dx.doi.org/10.1088/2040-8986/aaea54.

[227] P. Dhawan, M. Gaudig, A. Sprafke, R.B. Wehrspohn, C. Rockstuhl, Light-trapping structures for planar solar cells inspired by transformation optics, Opt. Express 29 (13) (2021) 19903–19919, http://dx.doi.org/10.1364/OE.426712, URL http://opg.optica.org/oe/abstract.cfm?URI=oe-29-13-19903.

[228] M. Sun, P.G. Kik, Scale dependent performance of metallic light-trapping transparent electrodes, Opt. Express 28 (12) (2020) 18112–18121, http://dx.doi.org/10.1364/OE.391351, URL http://opg.optica.org/oe/abstract.cfm?URI=oe-28-12-18112.

[229] M. Sun, P.G. Kik, Light trapping transparent electrodes with a wide-angle response, Opt. Express 29 (16) (2021) 24989–24999, http://dx.doi.org/10.1364/OE.431530, URL https://opg.optica.org/oe/abstract.cfm?URI=oe-29-16-24989.

[230] M. Sun, P. Golvari, S.M. Kuebler, P.G. Kik, Experimental demonstration of light-trapping transparent electrode geometries, ACS Photonics 10 (3) (2023) 595–600, http://dx.doi.org/10.1021/acsphotonics.2c01468.

[231] M.Q. Khokhar, S.Q. Hussain, M.A. Zahid, D.P. Pham, E.-C. Cho, J. Yi, Numerical simulation and experiment of a high-efficiency tunnel oxide passivated contact (TOPCon) solar cell using a crystalline nanostructured silicon-based layer, Appl. Sci. 12 (1) (2022) http://dx.doi.org/10.3390/app12010392, URL https://www.mdpi.com/2076-3417/12/1/392.

[232] C. Donolato, Effective diffusion length of multicrystalline solar cells, Semicond. Sci. Technol. 13 (7) (1998) 781, http://dx.doi.org/10.1088/0268-1242/13/7/021.

[233] M.J. Hossain, B. Tiwari, I. Bhattacharya, Novel high efficiency quadruple junction solar cell with current matching and quantum efficiency simulations, Sol. Energy 139 (2016) 100–107, http://dx.doi.org/10.1016/j.solener.2016.09.031, URL https://www.sciencedirect.com/science/article/pii/S0038092X16304376.

[234] P. Würfel, T. Trupke, T. Puzzer, E. Schäffer, W. Warta, S.W. Glunz, Diffusion lengths of silicon solar cells from luminescence images, J. Appl. Phys. 101 (12) (2007) 123110, http://dx.doi.org/10.1063/1.2749201.

[235] R.A. Pala, A.J. Leenheer, M. Lichterman, H.A. Atwater, N.S. Lewis, Measurement of minority-carrier diffusion lengths using wedge-shaped semiconductor photoelectrodes, Energy Environ. Sci. 7 (2014) 3424–3430, http://dx.doi.org/10.1039/C4EE01580K.

[236] M.J. Hossain, K.O. Davis, Photon management for silicon solar cells featuring hole-selective molybdenum oxide rear contacts: An optical simulation study, in: 2019 IEEE 46th Photovoltaic Specialists Conference, PVSC, 2019, pp. 1901–1905, http://dx.doi.org/10.1109/PVSC40753.2019.8981196.

[237] PV Lighthouse: SunSolve, URL https://www.pvlighthouse.com.au/sunsolve.

[238] M.J. Hossain, SunSolve_Reflectance_Eqe_J, 2023, http://dx.doi.org/10.6084/m9.figshare.23573409.v1.

[239] Y. Zou, X. Sheng, K. Xia, H. Fu, J. Hu, Parasitic loss suppression in photonic and plasmonic photovoltaic light trapping structures, Opt. Express 22 (S4) (2014) A1197–A1202, http://dx.doi.org/10.1364/OE.22.0A1197, URL http://www.opticsexpress.org/abstract.cfm?URI=oe-22-104-A1197.

[240] Y. Liu, T. Lai, H. Li, Y. Wang, Z. Mei, H. Liang, Z. Li, F. Zhang, W. Wang, A.Y. Kuznetsov, X. Du, Nanostructure formation and passivation of large-area black silicon for solar cell applications, Small 8 (9) (2012) 1392–1397, http://dx.doi.org/10.1002/smll.201101792, arXiv:https://onlinelibrary.wiley.com/doi/pdf/10.1002/smll.201101792.

[241] P. Repo, A. Haarahiltunen, L. Sainiemi, M. Yli-Koski, H. Talvitie, M.C. Schubert, H. Savin, Effective passivation of black silicon surfaces by atomic layer deposition, IEEE J. Photovolt. 3 (1) (2013) 90–94, http://dx.doi.org/10.1109/JPHOTOV.2012.2210031.

[242] W.-C. Wang, M.-C. Tsai, J. Yang, C. Hsu, M.-J. Chen, Efficiency enhancement of nanotextured black silicon solar cells using Al2O3/TiO2 dual-layer passivation stack prepared by atomic layer deposition, ACS Appl. Mater. Interfaces 7 (19) (2015) 10228–10237, http://dx.doi.org/10.1021/acsami.5b00677, PMID: 25919200.

[243] P.K. Parashar, S.A. Kinnunen, T. Sajavaara, J.J. Toppari, V.K. Komarala, Effective suppression of nanotextured black silicon surface recombination channels by aluminum oxide: comparison from sputtered and ALD grown films, Semicond. Sci. Technol. 36 (11) (2021) 115013, http://dx.doi.org/10.1088/1361-6641/ac2124.

[244] X. Liu, B. Radfar, K. Chen, T.P. Pasanen, V. Vähänissi, H. Savin, Tailoring femtosecond-laser processed black silicon for reduced carrier recombination combined with >95% above-bandgap absorption, Adv. Photonics Res. 2100234, http://dx.doi.org/10.1002/adpr.202100234, arXiv:https://onlinelibrary.wiley.com/doi/pdf/10.1002/adpr.202100234.